REPORT DOCUMENTATION PAGE

AFRL-SR-BL-TR-98-

0226

1. AGENCY USE ONLY (Leave blank)	2. REPORT DATE	3. REPORT TYPE AND DATES COVERED
		FINAL 15 Jan 94 To 14 Jul 97

4. TITLE AND SUBTITLE
CARBONACEOUS DEPOSIT FORMATION FROM ADVANCED FUELS UNDER SUPERCRITICAL CONDITIONS

5. FUNDING NUMBERS
F49620-94-1-0085
2303/DS
61102F

6. AUTHOR(S)
DR LISA D. PFEFFERLE

7. PERFORMING ORGANIZATION NAME(S) AND ADDRESS(ES)
DEPT OF CHEMICAL ENGINEERING
UALE UNIVERSITY
P.O. BOX 8286YS
NEW HAVEN CT 06520-8286

8. PERFORMING ORGANIZATION REPORT NUMBER

9. SPONSORING/MONITORING AGENCY NAME(S) AND ADDRESS(ES)
AFOSR/NL
110 DUNCAN AVE ROOM B115
BOLLING AFB DC 20332-8050

MAJ HUGH C. DE LONG

10. SPONSORING/MONITORING AGENCY REPORT NUMBER

11. SUPPLEMENTARY NOTES

19980310 091

12a. DISTRIBUTION/AVAILABILITY STATEMENT

Approved for public release;
distribution unlimited.

DTIC QUALITY INSPECTED 3

13. ABSTRACT *(Maximum 200 words)*

Methods for measuring speed of sound and heat transfer coefficients in supercritical reacting fluids were developed and tested. These measurements were used to show that relationships for predicting supercritical fuel properties near the critical point are not valid and that in-situ measurement is important. Measurement of reaction products from the thermal stressing of MCH over a wide range of pressures and temperatures with and without oxygen contamination shows that 1) dissolved oxygen is important in the formation of products in the bulk phase 2) insoluble residues from hydrocarbons at temperatures less than 850K are likely caused by the presence of oxygen and/or an active surface 3) the only aromatic species observed at low temperatures was toluene and naphthalene production can proceed through reactions of the benzly radical 4) the coating of the wall of the supercritical fuel reactor with catalytically inactive titanium nitride prevented significant surface activity. Deoxygenation and passivation of metallic surfacs can be used in actual aircraft ssytems to reduce deposit formation. Prevention of hot-spots is also critical as rupture of the MCH ring can quickly produce benzene and higher mass aromatics.

14. SUBJECT TERMS			15. NUMBER OF PAGES
			16. PRICE CODE
17. SECURITY CLASSIFICATION OF REPORT (U)	18. SECURITY CLASSIFICATION OF THIS PAGE (U)	19. SECURITY CLASSIFICATION OF ABSTRACT (U)	20. LIMITATION OF ABSTRACT (UL)

AFOSR Final Report, August 1, 1997

Grant #F49620-94-1-0085

Carbonaceous Deposit Formation From Advanced Fuels Under Supercritical Conditions

Theodore Randolph, University of Colorado
Lisa D. Pfefferle, Yale University

Grantee Institution Address: Yale University
Department of Chemical Engineering
P.O Box 8286YS
New Haven, CT 06520-8286

Table of Contents

Carbonaceous Deposit Formation From Advanced Fuels Under Supercritical Conditions

AFOSR Final Report, August 1, 1997

Grant #F49620-94-1-0085

Carbonaceous Deposit Formation From Advanced Fuels Under Supercritical Conditions

Theodore Randolph, University of Colorado

Lisa D. Pfefferle, Yale University

Objectives:

1. To develop techniques to measure supercritical fuel properties in-situ under reaction conditions. This is important because as the mixture reacts and the species composition change, the critical properties also change. Knowing where you are with respect to the critical point is important for data evaluation. This information is also needed to understand whether fuel reactivity or changes in product solubility are controlling changes in deposit formation near the supercritical point.

2. To understand the pyrolytic decomposition and subsequent hydrocarbon growth mechanisms of methyl cyclohexane (MCH) and how they are affected by supercritical conditions.

Summary of Results

For advanced engine and heat exchanger design, it is essential to know the critical points of the fuel and fuel-product mixtures. Ultrasonic velocity measurements provide critical point information and can also be used to obtain compressibilities. A novel system has been designed, constructed and used to measure velocities of sound up to 675K and 300 bar inside a large scale chemically reacting system. A quartz crystal was used to generate and receive the ultrasonic waves. Methylcyclohexane was used as a model for new endothermic fuels and critical points have been measured for methylcyclohexane and mixtures of methylcyclohexane and benzene. Experimental velocities and critical points were compared to values calculated from a Benedict-Webb-Rubin equation of state, corresponding states principle and mixing rules.

Sampling and analysis of supercritical fuel mixtures has also been carried out. Self-cleaning nozzle designs have been built and tested in heavily sooting diffusion flames and in the supercritical fuel reactor. Detection and quantification of unsaturated large hydrocarbons as well as oxygen-substituted products at concentrations below the parts-per-million range was demonstrated. Factors influencing the transit/detection efficiencies of large hydrocarbon species sampled from diffusion flames were studied, and thermophoresis found to be a major cause of sampling non-uniformities. Analysis of a large number of samples from the deoxygenated methylcyclohexane fuel used in the joint reaction/ultrasound velocity measurement studies discussed below showed that no higher hydrocarbon production and no oxygenated products were formed. Only minimal dehydrogenation was observed at the highest temperatures. Reaction was carried out at 575-625K and pressures from atmospheric to traversing the critical point. The fuel was deoxygenated prior to use. Other experiments showed that even with 100-300 ppm oxygen, significant fuel reaction does not occur until about 875-975K in the gas phase at 1-5 bar and 50-100ms residence time. These results are consistent with the very high pressure results suggesting that the reaction mechanism is not a strong function of pressure.

A second set of experiments under near supercritical conditions were carried out using heated wires to evaluate surface effects on higher hydrocarbon production. Little deposit was observed on any surface when oxygen had been removed to below ppm levels prior to the experiments until the wire temperature was increased to 775K. Heat transfer calculations in this system as measured by the power required to maintain the wire at a fixed temperature are described below. Deposit formation was observed as the wire temperature was increased above the reaction temperature accompanied a decrease in the measured heat transfer coefficient.

Because no higher hydrocarbons were observed in the bulk, deposit formation is likely a heterogeneous process.

Accomplishments/New Findings

1. A theoretical basis for analyzing reactivity in supercritical systems has been further developed and tested

2. Speed of sound measurements were made in deoxygenated methylcyclohexane and methylcyclohexane plus benzene across the critical point. A model for predicting the mixture critical point was shown to be in good agreement with the data.

3. Under these conditions (575-625K and pressures traversing the critical point) no higher hydrocarbon or decomposition was observed in the bulk emphasizing the importance of oxygen and/or surface mechanisms in these mechanisms at lower temperatures.

4. Significant higher hydrocarbon growth does not occur in the bulk phase until the MCH decomposition becomes fast. This can be accelerated by hot spots and/or surface effects.

5. A new naphthalene growth mechanism involving addition of C3 species to benzyl radical is possibly important in these systems at low temperatures.

6. Rate parameters for methylcyclohexane decomposition are not a strong function of pressure at least far from the critical point.

7. A method for determining heat transfer coefficients and evaluating surface deposit formation has been used based on hot wire anemometry. This has yielded heat transfer coefficients for clean wire conditions.

8. Conditions for deposit formation on metallic surfaces have been quantified. Coating surfaces with titanium as in our reactor inhibits deposit formation at all conditions tested in this study.

1. Computational and Theoretical Approaches to Understanding Reactivities in Supercritical Fluids Computational and Theoretical Approaches to Understanding Reactivities in Supercritical Fluids

1.1 Introduction:

The choice of solvent is of vital importance in the rational design of any reaction system. The large compressibility of a supercritical fluid enables wide variation in solvation with modest changes in temperature and pressure. In the case of reactivities in supercritical jet fuels, these changes in solvation may influence reaction pathways, both undesired (e.g., coking or carbonaceous deposit formation) or desired (dehydrogenation of methylcyclohexane in endothermic fuel applications). This has spurred our study of reactions in supercritical fluids. However, there is a lack of the fundamental understanding of the solvent effects of supercritical fluids on chemical reactions.

The molecular structure of supercritical fluid mixtures has received much recent attention. Specifically, there has been a focus on the phenomenon of local density augmentation of solvent molecules around solute molecules present at near-infinite dilution, and of local density augmentation of solutes around other solute molecules. Several spectroscopies (UV [1,2], photo ionization [3,4], fluorescence [5,6] and EPR[7]) have shown that such local density effects exist. Further evidence has been provided by integral equation theory [8,9] and molecular dynamics simulations [10] of supercritical fluid systems.

Such solvent-solute and solute-solute excesses could be expected to influence reaction rates. Yet experiments do not always show this to be the case. Both solvent-solute and solute-solute local density enhancement effects have been observed in some, but not all, reaction studies to date [11,12,13,14,15,16]. We have attempted to provide a microscopic understanding of the effect of local densities (both solvent-solute, and solute-solute) on rapid bimolecular reactions by comparing molecular dynamics and brownian dynamics simulations of an infinitely fast reaction that models Heisenberg spin-exchange, and electron paramagnetic resonance (EPR) spectroscopic studies of the same reaction.

1.2 Techniques:

Heisenberg spin-exchange is a rapid bimolecular reaction in which radicals possessing opposite spin states exchange spins by colliding with each other. More details of this reaction can be found elsewhere [17]. In our group, EPR studies of spin-exchange between di-tert-butyl nitroxide (DTBN) radicals in near-critical and supercritical ethane have been carried out [18]. In

our simulations, both DTBN and ethane were approximated as spherical molecules each possessing Lennard-Jones (L-J) size and energy parameters σ and ε respectively. O'Brien and co-workers have estimated the L-J parameters for DTBN [19], while the L-J parameters of ethane are readily available in the literature [20].

NVE molecular dynamics (MD) and equilibrium brownian dynamics (BD) simulations of DTBN in ethane were carried out over a wide range of densities. Details of these simulations are given elsewhere [19,21]. All parameters were made dimensionless using solute L-J parameters [22]. All simulations were carried out at a reduced temperature of Tr=1.084 (which corresponds to a dimensionless temperature T*=0.6336 in solute L-J units).

Local solvent-solvent, solute-solvent and solute-solute density enhancements estimated by applying the Percus-Yevick closure to the Ornstein-Zernike equation [24] at a reduced density of 0.6 are illustrated in Figure 1. There is significant enhancement for all three cases, but the solute-solute enhancement is the largest. Also, the local density enhancement is largest at a value of the collision length scale r* not much different from the solute L-J radius, suggesting that such enhancements should significantly affect the rate of those reactions whose cybotactic length-scale is comparable to the Van der Waals radius of the reactants.

1.3 Computational Results:

In our simulations, we considered the case of a reaction with infinitely fast kinetics in which every collision results in reaction. We probed the influence of solvent-solute clustering on the rate of solvent-solute collisions in a non-reacting environment. Solute-solute local density effects on collision and reaction rate constants were studied. In addition, we measured the lifetimes of collisions between solutes over a wide density range. In our simulations, we have defined a collision as occurring when two colliding molecules reach a specified distance R_c* from each other. By varying this encounter distance, we have estimated quantities of interest both as a function of density and of collisional length-scale. The rate constant for solvent-solute collisions was normalized by the gas kinetic limit and was plotted as a function of the collision radius for three different densities as shown in Figure 2. It can be seen that this ratio is quantitatively equal to the solute-solvent radial distribution function $g_{12}((r)$. Thus, for collision length-scales not very different from the Van der Waals radius, the rate of solvent-solute collisions is strongly influenced by the local solvent density. For large collision radii, however, the radial distribution function decays to unity and the collision rate is unaffected by local density effects.

Reaction rate constants were estimated as a function of density and collision radius. To test the radial dependence of the reaction rate, the rate constant normalized by the kinetic theory result is plotted against the collision radius as shown in Figure 3. At the lowest density, the normalized reaction rate constant falls on the line from kinetic theory predictions for the smaller collision radii. At the intermediate density, it differs from both the values from kinetic theory and from the Smoluchowski theory, while at the highest density, it is well-predicted by the Smoluchowski theory. This is reasonable since at high densities, the equilibrium radial distribution function is destroyed by reaction faster than it can be restored, and hence the reaction rate is unaffected by local structural effects. At the low densities however, the time required for the molecules to diffuse into their collision spheres is large compared to the time required for the fluid to relax into its equilibrium structure and hence the effect of $g_{22}(r)$, the equilibrium solute-solute radial distribution function is clearly seen.

However, no such variations are seen for the rate constants for solute-solute collisions which are also shown in Figure 3 normalized by the gas kinetic limit. As can be seen, these collision rate constants are exactly predicted from the modified kinetic theory over all density ranges. Collision rates are always influenced by the equilibrium solute-solute radial distribution function $g_{22}(r)$ since non-reactive collisions do not influence the equilibrium structure of the fluid.

1.5 Comparison with EPR Measurements:

The materials and methods used to carry out EPR spectroscopic measurements of spin-exchange are described elsewhere [18]. Reaction rate constants measured as a function of density from the BD simulations for a collision radius of $r=1.0\sigma_{22}$ are plotted alongside the rate constants from EPR as shown in Figure 4. It can be seen that the rate constants qualitatively resemble each other. To provide a quantitative comparison, two quantities are needed: a). The cybotactic radius for spin-exchange and b). The reaction probability. The cybotactic length scale for spin-exchange is estimated to be between one and three hard sphere diameters [29]. The reaction probability is a function of the lifetime of collisions between reactants, with an upper bound of 1/2 [18]. Note that the computationally determined rate constants assume a reaction probability of unity.

One of the keys to understanding solvent structural effects on reactions is to know what the real collision length-scale required for reaction is. Quite obviously, different reactions have different collision length-scales; based on our results therefore, the effect of local densities on different reactions is different. To predict and understand the kinetic effects of solvents by

comparing and contrasting the various experimental studies of reactions, it is essential to have precise quantitative estimates of the collision length-scale required for all of the reaction systems being studied.

1.6 Collision Lifetimes:

We measured the lifetimes of individual solute-solute collisions in BD simulations over the reduced density range from 0.1455 to 1.455 for a collision radius of r=1.57 σ_{22}. Collision lifetime distributions obtained, as shown in Figure 5, are strongly density dependent. At the intermediate densities the lifetimes are distinctly bi-modal. Note that the distributions have been normalized such that the integral of each distribution is unity.

For the purpose of illustration, we have marked as "A" and "B", the two peaks that appear in the lifetime distributions. At the lower densities, peak B is very prominent, while at the higher densities, it all but disappears and Peak A is dominant. At the low densities, when molecules move thermally rather than diffusively, the tendency to sit in each other's potential well is very strong since the effect of the mean field is small. Most collisions that occur at these densities are mediated by the intermolecular interaction, and this causes the single peak B in the lifetimes. This result is consistent with observations of gas-phase clustering which predict such trends in the collision lifetime [30].

At the higher densities however, it is the mean field interaction that is significant. This increases the duration of collisions. It can be seen from Figure 5 that the lifetime distributions at high densities exhibit long tails. Our observations are consistent with the first passage time results for estimating average survival lifetimes in diffusive processes [31].

The lifetime distributions may thus be thought to reflect the counteracting influences of the intermolecular potential and the mean field interaction. While the low density and high density effects on collision lifetimes are understood, the bi-modal behavior that occurs at the intermediate densities is not. The occurrence of the bi-modal region is due to the fact that neither the intermolecular force nor the mean field interaction clearly dominate at the intermediate densities. It is interesting to note that for reactions requiring collision length-scales that are not much larger than the hard sphere value, the density range where this bi-modal behavior occurs falls in the near- and supercritical region.

1.7 Conclusions for section 1:

The rate of solute-solvent collisions has been shown to be directly related to the radial distribution function $g_{12}(r)$. Even though this treatment was for transport-limited reactions, this result has implications for those reactions where the rate determining step is collisional-energy transfer between solvent and reactant [34]. It has also been shown that correlations in the radial distribution function $g_{22}(r)$ strongly affect solute-solute collision rates. They affect reaction rates only at the lower densities and for certain collision radii. We have also compared our rate constants from BD simulations with EPR spectroscopic measurements; the two sets of rate constants display the same qualitative trend as a function of density. Collision lifetimes estimated from the simulations display a strong density dependence. They are distinctly bi-modal at the higher densities and reflect the conflicting effects of the intermolecular force and the mean field interaction.

2. Experimental Investigations of Supercritical Fluid Speed of Sound Measurements, Fuel Stability and Transport Phenomena

2.1 Introduction/Summary:

The fuel in a high speed aircraft is the only practical coolant that can be used to absorb the excess heat from on-board sources. As the speed of the aircraft increases, the heat sink requirements for the fuel go up substantially. This implies that the fuel temperature must be raised to cool faster aircraft. But the hydrocarbon fuels now in use have an upper temperature limit which cannot be exceeded without chemical decomposition and formation of insoluble solid deposits that foul heat exchangers, fuel nozzles and cause disruptions in the fuel system [35,36]. Thus, it is imperative to develop fuels that can withstand higher heat loads. Fuels currently in use can withstand temperatures of 755 K without thermal decomposition; this would suffice for cooling aircraft up to around Mach 5 [34]. For greater speeds, additional cooling will have to be obtained by having the fuel undergo an endothermic reaction.

One hydrocarbon that is being investigated for use as an endothermic fuel is methylcyclohexane (MCH). The formation of toluene by the Pt-catalyzed dehydrogenation of MCH is an endothermic reaction that almost doubles the amount of heat that can be absorbed by the fuel without decomposition [37]. The combustion efficiencies of the reaction products are high.

Measurement of speed of sound in supercritical fuel mixtures serves at least two purposes relating to Air Force missions. First, the speed of sound is necessary for the design of mechanically durable fuel heat exchangers. Flow instabilities and heat transfer instabilities in fuel heat exchangers may prove to be a serious obstacle in designing new high-performance engines; this study provides fundamental data for proper heat exchanger design. Second, the speed of sound is linked to basic thermodynamic properties of fuel mixtures such as mixture critical points and heat capacities as a function of pressure, temperature, and mixture composition. The detailed circuit design is available for use in Air Force laboratories from Prof. Randolph.

High-Performance Aircraft Heat Exchanger Design:

To cool the airframe and aircraft components, the fuel has to circulate and exchange heat while undergoing endothermic reaction. The fuel temperature increases as it absorbs heat from the surroundings. For high heat loads, the fuel flow rate needs to be high to ensure adequate cooling. This means that the pressure in the tubes can exceed the critical pressure of the fuel. So the fuel can undergo a transition through its critical point from a subcritical to a supercritical state as it flows in the heat exchanger.

Sharp increases in the heat transfer coefficient just above the critical pressure have been reported for water [38]. In an investigation of heat transfer to hydrocarbon fluids flowing in round, thin walled electrically heated tubes, Hines and Wolf [39] observed a similar effect when the wall temperature exceeds the critical temperature and pressure is close to the critical pressure of the fluid. There is also a vibration which accompanies this increase in heat transfer. This vibration is strong enough to damage or even rupture the tubing. When the pressure is much higher than the critical pressure, there is no vibration or an increase in the heat transfer. This indicates that the anomalous behavior is purely a critical phenomenon. Pressure oscillations have been detected near the critical point while studying heat transfer to Jet A fuel [40].

Since the fuel undergoes endothermic reaction as it passes through the heat exchanger tubes its composition, and hence critical properties, change. For the design of a stable heat exchanger, it is essential to know the critical properties and thermodynamic properties of the pure hydrocarbon and the hydrocarbon product mixtures. The velocity of sound tends to zero as the critical point is approached, so it can be used to locate the critical point. When coupled with density measurements, velocity measurements can be used to calculate isothermal, isentropic compressibilities and the ratio of specific heats [41], quantities which are essential for engine and heat exchanger design. Velocity of sound measurements have been used to study supercritical

fluids [42-49] and recently a miniaturized system with lead zirconate-lead titanate transducers has been used to determine critical points of pure substances and mixtures [50,51].

Summary of work in Section 2:

The mixture critical point for a methylcyclohexane-based fuel undergoing endothermic dehydration reactions is strongly depends on the degree of conversion of the reaction. Other fluid properties of interest are also highly dependent on the degree of conversion of the reaction. For example, the speed of sound in a fuel mixture depends not only on the temperature and pressure of the fuel, but also on the fuel's composition. Speed of sound measurements were carried out in both methylcyclohexane and methylcyclohexane/benzene mixtures across the critical points to assess mixture effects. At the conditions tested no higher hydrocarbon or oxygenated species were observed. Slight amounts of fuel dehydrogenation was observed. The ultrasound technique development proved the most challenging due to the low piezoelectric strain constant of quartz, which has discouraged others from using this technique at high temperatures in the past. We have developed the circuitry and a novel pulse transformer to make this technique workable.

As discussed in the 9/95 report, no conventional design can operate both at the high temperatures and pressures of interest in this work. To measure speeds of sound in liquids, piezoelectric transducers are made from PZT (lead zirconium titanate) or lithium niobate. Unfortunately, both of these common transducer materials have Curie temperatures (the temperature above which the spontaneous polarization and hence the piezoelectric properties are lost) that are too low for our application. PZT and lithium niobate have upper operating limits of around 575K and 425K, respectively. Thus, it was necessary to design new sensors based on quartz, which has a Curie temperature around 875K and an effective maximum operating temperature around 825K. Besides its high Curie temperature, quartz also offers low chemical reactivity. Quartz, however, is an inconvenient piezoelectric material, because of its low piezoelectric strain constant of about 2.3 E^{-12} m/volt. This means that electrical pulses of 1000 volts only generate a displacement of about one nanometer. Our design to overcome the difficulties inherent to the use of quartz as a piezo-electric material are discussed below and in more detail in our 9/95 report.

In the section below, a system to make acoustic measurements and thermal stability analysis at high temperatures and pressures is described with results for MCH and MCH - benzene system along with a description of the supercritical reaction system and results for fuel stability and deposit formation. Chemical mechanisms are discussed in section 3 below.

Velocity of sound measurements in compressible fluids at high temperatures and pressures pose special challenges. For this application (examination of fuel mixtures near the critical point), it is necessary to construct an apparatus that will be able to make velocity measurements at temperatures up to 625-675K. These high temperatures constrain the piezoelectric material that can be used to generate acoustic waves as discussed above. The temperature also restricts the materials that can be used in the construction of the pressure vessel due to sealing problems. At these temperatures, the fluids of interest can react and form products which will alter the velocity and the critical points, especially when catalyzed by metal surfaces. To minimize catalytic effects of the vessel surface, passivating ceramic coatings were applied to all exposed metal surfaces.

2.2 Materials and Methods:

The chemicals used were methylcyclohexane (Aldrich, 99%, spectrophotometric grade) and benzene (Fisher, infra-red spectra analyzed). The critical temperatures of the fluids and mixtures investigated are around 575K, and at these high temperatures, the fluids can oxidize and cause deposition. To minimize oxidation, MCH and benzene were deoxygenated before use. For pure MCH, this was accomplished by filling the vessel with the desired amount of MCH, then boiling it in the reactor at atmospheric pressure. The vapors were allowed to condense in a transparent tube and then collected in a flask. This was continued till no air bubbles could be seen coming out of the reactor into the condensate. For the MCH- benzene mixture, the two were degassed separately before mixing. Degassing was achieved by boiling in a stoppered conical flask with a tube attached to the outlet till the vapors reached the top of the flask and liquid started gushing from the outlet. In all cases, mass spectrometric analysis of the fuels after several days at supercritical conditions showed that neither oxygenated products nor oxygen itself could be detected.

Velocity of sound measurements were made at constant temperatures over a large range of pressures traversing the critical point (25-80bar, Fig. 8). This was done be heating the reactor with the fluid inside to the desired temperature. The final pressure reached was the highest pressure at which measurement was taken. The pressure was then slowly lowered by opening the valves for a controlled leak. When the pressure reached the desired value, the valves were closed and a measurement taken after the pressure reading stabilized. This was repeated till a minimum in the velocity was obtained. The temperature could be controlled with an accuracy of 1K. Thermal stability tests were performed on deoxygenated MCH. MCH was held at a constant temperature and samples were withdrawn at regular intervals and analyzed. The pressure varied by 2-3 bar over a period of 24 hr. This test was repeated at two temperatures, at 575K (very close to the critical temperature) and at 625K (supercritical region).

2.3 Velocity measurement technique:

The ultrasonic velocity is measured by the pulse-echo method. The block diagram of the circuit is shown in Figure 6. The transmitter circuit sends synchronous pulses to the sawtooth generator and to clear the counter. This pulse also causes a current to flow through the transformer which applies a high voltage across the faces of the transducer in a spike of about 4 μs duration. The transducer starts oscillating at its resonant frequency and these oscillations travel through the medium and reach a similar transducer on the other end which sends out electrical signals when excited by the ultrasonic waves impinging on it. These signals are amplified and sent to an oscilloscope. The sawtooth pulse and the output of a manually adjustable potentiometer are sent to a comparator which shuts off the counter. The potentiometer is adjusted by looking at the scope so that the lagging edge of the timing pulse coincides with the leading edge of the signal from the receiver. The counts are read into a computer and converted to time.

The piezoelectric transducer is a quartz crystal. For quartz, the Curie temperature is 848K and the maximum operating temperature is around 675K. Quartz is the only piezoelectric material with operating temperatures high enough to be used in the critical region of the fluids of interest. Quartz is also chemically inert. The quartz crystals used have a natural frequency of 250 kHz. The crystals have been obtained from Valpey-Fisher.

Quartz has a very low piezoelectric strain constant (ca. 10-12m/volt). The piezoelectric strain constant is the ratio of the change in thickness (strain) to the applied voltage. This implies that very high voltages (of the order of several thousand volts) are needed to produce enough deformation in the quartz crystal to get any significant output of ultrasonic waves in the medium. For maximum coupling of the electrical pulse to the mechanical deformation pulse, the pulse should be delivered at the characteristic resonance frequency of the transducer (the natural frequency of oscillation of the quartz crystal). Our quartz transducers have a 250 kHz resonant frequency, which requires 4 microsecond pulses. To deliver these 4 microsecond long, 10,000 volt pulses we have designed a custom pulse transformer. Conventional pulse transformers tend to "ring" for a relatively long time after each pulse. Such echoing generates noise making detection difficult. To circumvent this, we built a transformer with a soft "lossy" iron core. The iron core damps the circuit fast enough so that the pulse is essentially composed of a single, bipolar spike versus ground. The front face of the gold-sputtered quartz transducer is maintained in electrical contact with the grounded stainless steel reactor body, while the back face is connected via the ceramic-coated feedthrough to the transformer or detector circuit. This scheme makes certain that the detector and transmitter share a common ground, and helps to eliminate

ground-loop problems. A driving circuit and matching detection circuit allow us to make speed of sound measurements at 100 Hz. A block diagram of the circuit used to measure the velocity of sound is given as Figure 6.

2.4 Reactor design:

The ultrasound vessel is made of 316 stainless steel and has a working volume of approximately 1.8 liters. The inner diameter of the reactor is 7.1 cm. The large diameter leads to a small surface to volume ratio. This reduces the surface for any reactions that can occur at the wall. To reduce further catalytic effects, exposed metal surfaces of the vessel were coated with a ceramic diffusion barrier. All tubular surfaces were coated with titanium nitride by Surface Solutions, Inc. using a DC linear magnetron sputtering technique. In this technique, a water-cooled tubular titanium cathode is placed internal and coaxial to the tubular stainless steel substrate on which a coating is desired. The magnetic field necessary to contain the plasma during the sputtering is achieved by electrically generating a circumferential magnetic field along the entire length of the target. Coating uniformity is ensured by effecting a constant plasma thickness that is uniformly excited along and over the entire length of the plasma target. This is achieved by the plasma drift current, running in the plasma circumferentially surrounding the target and parallel to the axis of the target. To form the inert ceramic surface, a reactive sputtering technique is employed. Nitrogen is bled into the system during sputtering of titanium to form a continuous, high density ceramic coating of titanium nitride. Non-tubular surfaces in the reactor were passivated using a different coating technique. Stabilized alumina was flame-sprayed onto the surfaces, followed by a second alumina coating and densification step at high temperatures.

The electrical feedthrough must operate at high temperatures, withstand high voltages and seal high pressures. A vacuum feedthrough from Insulator Seal Inc. has been modified to be able to seal pressures up to 10 MPa. The feedthrough is rated at over 5000 V but not exceeding 12000 V and a temperature of 725 K. The feedthrough assembly is shown in Figure 7. To strengthen the thin metal sleeve, a stainless steel bushing is inserted between this and the ceramic insulator. Sealing is achieved by a silver coated stainless steel O-ring that seats on the other end of the metal sleeve. The O-ring is compressed by tightening the nut onto threads cut on the inside of the cavity housing the feedthrough. This nut pushes against the lip of the bushing and compresses the O-ring. The reinforcing of the sleeve is so that the thin metal sleeve does not buckle under the compression of tightening this nut.

2.5 Results and Discussion Speed of Sound Measurements:

The velocity of sound in MCH and MCH-benzene mixtures has been measured as a function of pressure at temperatures in the vicinity of the critical temperature. The critical point is taken to be the point of the minimum velocity of sound, since high attenuation near the critical point makes it impossible to observe velocities close to zero. Figure 8 shows a typical isotherm. The calculated velocity of sound values have been obtained from the Benedict-Webb-Rubin equation of state for pentane and a corresponding states equation for MCH using the formula [52]:

$$V = [(Cp/Cv)*(\delta p/\delta \rho)T*10^6/M]^{0.5} \qquad [1]$$

Cp, Cv are evaluated from the BWR/corresponding states equation, M is the molecular weight and (is the density.

The experimental and calculated sound velocities differ by about 3% away from the critical region but this difference increases to as much as 25% very close to the critical point. This is because the equation is inaccurate close to the critical point and hence does not predict the quantitative drop in velocity. The velocity of sound in the critical region of MCH is presented in Figure 9. There is no one minimum in the velocity that is much lower than the others but there are two comparable minima. The true critical point has to lie between the two minima. So the arithmetic mean of the temperatures and pressures at which the minima occur is taken as the critical point.

The critical points for pure fluids MCH and benzene have been obtained from literature [53]. The critical temperatures of the mixtures have been evaluated by a simple mole fraction method and the critical pressures by the modified Prausnitz and Gunn combination as indicated in Reid, et al., (1987). The critical points have also been determined using the second virial coefficients for the mixture [53]. These are shown by the dotted and the full line respectively and compared with the experimental values in Figure 10. The measured Tc and pc of MCH, including the error bars, are respectively within 0.33% and 3.75% of the reported values. It can be observed from Figure 10 that the values obtained with the second virial coefficients coincide with the experimental data except in a 50-50 mixture of MCH and benzene which has a lower pc than predicted.

The critical behavior of the mixture observed experimentally also matches the qualitative predictions made earlier. Benzene and MCH have critical properties that are comparable in magnitude and are chemically similar, so they form a type I mixture where they are fully miscible and have a continuous gas-liquid critical line which is concave and extends from the critical point of one component to the other [54]. This is also true of most of the MCH dehydrogenation products which are formed under fuel stressing prior to fuel decomposition.

2.6 Thermal Stability Testing:

When the MCH fuel was deoxygenated, the results of the thermal stability tests indicated that there was no significant formation of products in any of the runs discussed above. To further test the thermal stability of the MCH, the fuel in the reactor was held for 24 hours at 30 bar and two different constant temperatures, one near 575K and one above 625K, the critical point of the fuel. Fuel samples were analyzed at regular intervals by mass spectrometry. No decomposition products were observed even after the full 24 hour run at both temperatures. Small (ppm) levels of dehydrogenation products were observed. Dehydrogenation products may be important to heterogeneous deposit formation if the appropriate metal surfaces are present. As discussed below the presence of oxygen enhances the formation of dehydrogention products at lower temperatures. Only toluene was observed at low temperatures. Benzene only becomes the predominant dehydrogenation product at high temperatures where significant MCH ring decomposition occurs. No benzene was observed in any supercritical fuel run because as discussed below until 875-975K MCH ring decomposition is minimal.

The two likely main reasons for the observation of no higher hydrocarbon formation in the bulk are: 1) dissolved oxygen is important in the formation of products and insoluble residues from hydrocarbons at high temperatures and the deoxygenation of MCH before the stability tests prevented oxidative reactions from initiating product formation and 2) the coating of the wall of the reactor with catalytically inactive titanium nitride prevented significant surface activity. These strategies can be used in actual aircraft systems to reduce deposit formation.

2.7 Heat transfer coefficients and Deposit Formation on the Fine Wire Probe

Hot wire anemometry was used to provide an in-situ measurement of heat transfer coefficients in near critical and supercritical fuels. The system consisting of a rack of fine wires heated by electric resistance was employed to study both deposit formation and to measure heat transfer coefficients. Heat transfer rates can be determined from the power dissipated. The voltage needed to pass a given amount of current through the wire which is resident in the reaction mixture is measured. From known resistivities as a function of temperature, the surface

temperature of the wire can be computed. When combined with the measured power input to the wire, the heat transfer coefficient can be computed. By independently varying the bulk temperature of the fluid (which is not significantly affected by the thin hot wire), the density of the fluid and the surface temperature of the wire, we can generate heat transfer coefficients that span a wide range of conditions.

We have tested the system under subcritical non-deposit forming conditions. Here, our data is represented well by the standard correlation $Nu=1.09(GrPr)^{0.2}$, where Nu is the Nusselt number hL/k, Gr is the Grashof number $L^3*r^2*g*B*(T_{surface}-T_{bulk})/m^2$, Pr is the Prandtl number cp*m/k. Under the subcritical conditions tested no deposit formation was noted. The subcritical testing thus validates the technique.

Figures 11 shows the heat transfer coefficient in n-heptane measured by the hot-wire anemometry technique. The heat transfer coefficient to a copper wire in supercritical methyl cyclohexane was also tested (P_r= 1.15, T_r = 1.02) and found to be about 200 $W/m^2/K$ at a wire temperature of 615K. This technique is being refined and conditions extended in our follow-on ASSERT research.

2.8 Conclusions for Section 2:

A feasible system to make velocity of sound measurements in compressible fluids at temperatures till 675K and high pressures to has been constructed and tested. From these velocity measurements, critical points and, with density measurements, the compressibilities are evaluated. These quantities are invaluable for engine and heat exchanger design. Since there are no correlations that can accurately predict these quantities in the near critical and supercritical regime of the fuel, the *in-situ,* non-invasive acoustic method developed in this research is the most reliable technique. A system for measuring heat transfer coefficients and surface reactivity has also been developed and tested. Deposit formation in the bulk is not a problem for most realistic operating conditions if oxygen is removed and surfaces are passivated.

3. Mechanism for MCH decomposition and Higher Hydrocarbon Formation in the Bulk: VUV-Mass Spectrometric Measurements of Reaction Products

3.1 Introduction and Summary

MCH pyrolysis pyrolysis was studied under a wide range of conditions from 300Torr to straddling supercritical conditions. At very low pressures the initial steps were studied but at moderate pressure gas phase conditions radical reactions predominate. Significant higher hydrocarbon production at sub second residence times does not occur until temperatures well above the critical point where MCH conversion is significant. Oxygen and surface reactions can accelerate dehydrogenation processes at lower temperatures.

3.2 Experimental Techniques

The high pressure experiments were carried out in the reactor described in section 2. Low to moderate pressure (P<3 bar) pyrolysis of MCH was carried out in a microjet reactor. This reactor and analysis coupling are described in earlier work [55]. This is a miniature fast-flow reactor coupled directly to a sonic nozzle with a volume of approximately 4.5×10^{-8} m^3. The reactor geometry consists two sets of concentric alumina insulator rods inserted into a larger 3 mm i.d., one end closed alumina tube. The nozzles were laser drilled at the exit end (2-10 mm) to provide adequate gas load on the pumping system while operating at the desired microreactor pressures. The inner tube is positioned to leave a reaction chamber 22 mm in length. Reactant is introduced to the reaction zone through the .05 mm clearance between the tubes at rates varying from 0.1 - 1 SCCM for the experiments reported here. The pressure upstream of the reactor was maintained between 300 and 2280 torr. The MCH was diluted with argon with initial concentrations from 7000 - 10000ppm.

The reaction zone is resistively heated (25 mm long Ta wire coil) and the temperature is calibrated using .003" thermocouples. A radiative shield and cooling jacket were found to be essential to keep stable reactor temperatures. Cooling of the uppermost part of the 10 cm long outer alumina tube was use to protect the viton-teflon seals and to sharpen the temperature profile at the reactor. The microreactor was set up on an XYZ positioner to allow full flexibility on the location of the supersonic gas expansion within the ionization region. Under the flow conditions discussed the microreactor was shown to approximate a well-stirred reactor [56].

Reaction products are measured using VUV photoionization mass spectrometer (VUV-MS) for products with IP<10.5eV and EI quadrupole MS for high IP species. The VUV-MS is

equipped with Wiley-McLaren type acceleration for higher resolution and an Einzel lens to compensate for the normal component of kinetic energy so that the probability of reaching the detector is relatively independent of mass. The sample introduction, which is normal to the flight tube axis of the mass spectrometer, minimizes detector fouling from neutral species generated in the reactor, and decreases the width of the ion velocity distribution along the time-of-flight axis, resulting in higher resolution as compared with the on-axis arrangement. Additional detector protection is provided by a liquid nitrogen cryotrap. The detector sensitivity (microchannel plate type with wide linearity range) is not decreased after many months of operation with pyrolysis samples. Overall detector gain after linear amplification is estimated to be 10^8 and the response linear over three orders of magnitude. Ion signals are averaged (2000 traces of 50 ms record length at 10 Hz rate) in real time and recorded directly onto a 100 MHz digital storage oscilloscope which is interfaced with a PC for data analysis. The overall mass resolution for the experiments described herein was measured as 470 at 78 amu.

VUV photons were generated by the non-linear optical mixing technique of third harmonic generation in Xe. 355 nm radiation from a Nd:YAG laser (Quanta Ray DCR-3G system) operating at 10 Hz was focused into a Xenon cell at 7.5 Torr. Maximum 118 nm production as determined from benzene one photon ionization was found at approximately 40 mJ of energy in a 6 ns pulse at 354.6 nm, corresponding to a peak power of approximately 8.7 x 10^6 W. The spectra used here however are taken with 28 mJ of power where multiphoton processes and spurious effects from electrons generated at the vacuum chamber surfaces (through 355 and/or 118 nm radiation) were found to be completely absent. This is the advantage that can be taken by the use of a high sensitivity detector. In addition, multiphoton processes (118 + 355 nm) at the ionization region are minimized through differential focusing and the slightly off-axis entrance angle of the 355 fundamental. The positioning of the 118 focal point is controlled with an XYZ translation stage.

Ionization efficiencies at 118 nm are relatively constant (+/- 40%) and high for five carbon hydrocarbons and larger, since these compounds have ionization potentials (IPs) of one to two eV below the photon energy (1182 Å = 10.49 eV). Therefore the simultaneously-obtained peak ratios are good approximations of relative concentration. However for smaller hydrocarbons with ionization potentials lying closer to the single photon energy, absorption cross sections and ionization efficiencies vary considerably and individual calibrations are made. Since only masses are detected in this study, the identity of structural isomers can only be inferred from arguments of internal consistency or knowledge of kinetic mechanisms and rate constants.

Factors influencing the detection sensitivity of the higher hydrocarbon products expected in this research have been studied using flow reactor pyrolysis/oxidation of benzene and phenol and hydrocarbons including PAH measurements in near-sooting diffusion flames. A methane diffusion flame doped separately with benzene and toluene was used to study gas phase mechanisms for higher hydrocarbon growth from these starting single ring species. Factors governing transit/detection efficiencies of the large hydrocarbon species sampled from the diffusion flame were studied, and thermophoresis was found to play a major role in sampling non-uniformities.

3.3 Supercritical Conditions

Analysis of samples of deoxygenated methyl-cyclohexane at pressures from 34 to 49 bar and temperatures up to 675K showed no evidence for higher hydrocarbon growth or oxygenated products in any of the runs in the minute to hours residence time range. Only a small amount of dehydrogenated products were observed at the highest temperatures. These appear when trace oxygen is present in the fuel. Metallic surfaces (including our copper heat transfer probe) accelerate dehydrogenation to toluene. Toluene is the first and highest concentration aromatic species formed in these and lower pressure, low temperature experiments primarily through surface reaction but also at trace concentrations in the bulk. No benzene was observed at these conditions although it was noted as the largest concentration aromatic product at higher temperatures in the lower pressure experiments described below (ppm onset at 875-975K) . This confirms the observation that oxygen and/or catalytically active surfaces are necessary for significant reactivity to occur at temperatures and pressures near the critical point. The conditions of the experiments at Yale were those used in the ultrasonic velocity measurements reported by Natarajan and Randolph at the University of Colorado as discussed above in the same reactor.

3.4 Reaction Mechanisms:

In separate experiments over a range of lower pressures (300-2280torr) we found that significant reaction of methylcyclohexane does not occur until 875K-975K for 50-100ms mean residence time. When compared with the data of Brezinsky (Eastern States Combustion Institute Meeting, WPI, 1995) taken at pressures far above the critical point, and our measurements near and well below the critical point (see below), the rate parameters for methylcyclohexane conversion are found not to be a strong function of pressure. We expect any modification in reactivity to be particularly important only near the critical point emphasizing the importance of *in-situ* property measurement in the reactor as developed in this study. This finding also

suggests that relative solubility effects may play the controlling role in determining differences in deposit formation near the critical point.

Figures 12-21 show products from MCH pyrolysis (approx. 7000ppm in Ar) at 760torr and 150ms (12-14), 50ms (15-17) and 1400torr and 45ms (18-20). Remember that these are well-stirred reactor experiments so each point on the graph represents a different reactor run and a slightly different starting concentration. The C2 products quickly predominate with ethylene greater than 90% of the C2 total (acetylene appears at the highest temperatures). In all cases mass 83 (see figures 13, 16 and 19) was the first intermediate observed as temperature was increased. At the highest temperatures benzene was the predominant aromatic species observed (see figures 14, 17 and 20). As expected from the apparent activation energy described below, increasing the residence time by a factor of 3 in this temperature range decreased the temperature for an equivalent conversion by approximately 40-45K but did not change the order of products observed. Also as expected peak intermediate concentrations were somewhat lower in the longer residence case due to the lower temperature and thus slightly slower MCH decomposition rate. The runs at the two different pressures show almost identical MCH decay profiles. The profiles for intermediates are also very similar. The only difference that is outside of measurement error is a broader peak at a slightly lower peak concentration for butadiene and earlier increase in C2 products. Higher hydrocarbons formed were the same in all cases run with the naphthalene the predominant 2-ring species observed. Benzene was the largest concentration single ring species observed followed by toluene, styrene and phenyl acetylene. Other higher mass species observed at the highest temperature at ppm levels included dihydronaphthalene (mass 130), methylnaphthalene (mass 142) , biphenyl (mass 154), fluorene (mass 166) and masses 152,166 and 178.

In Table 1 below, the "+" represents that the species were first detected at ppm concentrations at the corresponding temperature for low pressure runs at 50 ms by our VUV and EI mass spectrometers. The progression of species observed was the same for all of the conditions run (500-1200K) but the temperatures are shifted.

Table 1 qualitative information about the process of MCH pyrolysis

Temperature ,K	*713*	*863*	*901*	*944*	*983*	*1093*
methane CH_4		+				
acetylene				+		
ethylene C_2H_4		+				
propene C_3H_6				+		
allene C_3H_4					+	
1,3-butanene			+			
AMU=52					+	
AMU=55					+	
AMU=56		+				
AMU=66					+	
isoprene, C_5H_8		+				
AMU=69		+				
AMU=70		+				
benzene C_6H_6*					+	
AMU=80					+	
AMU=82	+					
AMU=83	+					
toluene		+				
AMU=94		+				
AMU=96		+				
AMU=102						+
AMU=104						+
AMU=116						+
AMU=128						+

*above 983K benzene is the major aromatic product.

From table 1, we can see that the first intermediate at the lowest temperature is AMU=83, which is cyclohexyl. From these observations we can show that one initiation step for MCH pyrolysis is $C_6H_{11}CH_3 \rightarrow C_6H_{11}+CH_3$ (R1). Brown and King [57] have carried out an RRKM analysis of the first steps in MCH pyrolysis and concluded that at 1100K the rupture of the C-C bond in the ring adjacent to the methyl group accounted for 70% of the MCH disappearance. Although our overall rate constant measured at 300torr is consistent with that reported by Brown and King. we see more methane than can be explained if R1 is a minority reaction channel. We cannot however measure the direct ring opening products because they are at the same mass as MCH. Masses 96, 94, 93 and 92 are measured with mass 96 peaking at the lowest temperature and 92-94 increasing leveling off and then increasing again with temperature consistent with formation of linear and then ring to aromatic species. Toluene was measured in these runs and in some SCF runs at temperatures below benzene. At the lowest end of the temperature range (500-650K) toluene production was greatly enhanced by the addition of metallic surfaces and/or oxygen. Benzene is not appreciably formed by dehydrogenation of the cyclohexyl radical . Compared with cyclohexyl radical (AMU 83), the concentrations of cyclohexene or linear C_6H_{10} (AMU=82) and C_6H_{12} (AMU=84) remain at a very low concentrations along with consequent dehydrogenation products. These species are rapidly converted to C2-C4 products with ethylene production predominant as discussed below. This suggests that much of the benzene formed is from recombination of C2-C4 precursors formed as MCH decomposition products.

Table 2 shows rate constants determined in this study and by other researchers for the overall disappearance of MCH in pyrolysis at moderate temperatures. Brown and King [57] used a triple aperture very low pressure reactor to determined the overall homolysis rate for MCH. The activation energy they measured for the sum of the channels (350kJ/mol) is close to that of the carbon-carbon bonds in MCH indicating that secondary radical reactions were indeed unimportant. In our low pressure studies (300 torr, microreactor) an activation energy of 365kJ/mol was measured again close to that of the carbon-carbon bonds in MCH. This again indicates that secondary radical reactions were unimportant and that the ceramic surface did not change the mechanism. The overall rate constant we measured was somewhat higher but consistent with that of Brown and King.

Table 2 Comparisons of kinetic parameters for MCH pyrolysis from different researchers

	Zeppieri etc. [4]	**Kralikov etc. [3]**	**Brown etc. [1]***	**THIS STUDY**
Reactor	Princeton Turbulent Flow Reactor	Steel Tube reactor	Triple-Aperture Reactor	Ceramic Microjet Reactor
Pressure(torr)	760	760	very low	300 (1-5bar)
Temperature(K)	1050-1200	970-1095	861-1218	500-1110 (-1150)
$k^0(s^{-1})$	$3.7\pm0.5X10^{13}$	$6.31x10^{15}$	$6.1x10^{16}$	$2.4x10^{17}$ ($5\text{-}7x10^{13}$)
E(kJ/mol)	265±5	251.2	350±10	365.15 (245-280)
Conce. profile	ethene>1,3butadiene> methane>propene	methane>ethene> propene>1,3 butadiene		ethene>methane> 1, 3 butadiene> propene>isoprene

*rate reported here is sum calculated for all postulated reaction channels

At higher pressures in the microjet reactor experiments the *apparent* activation energy for MCH decomposition decreases indicating the increasing importance of secondary reactions involving H radical reaction. Kralikov et al. carried out the MCH pyrolysis reaction in a stainless steel tube at temperatures around 1000K. Their measured apparent activation energy was low and overall rate constant significantly higher than in other measurements likely due to surface reactions. The mechanism was also affected by possible surface reactions as these investigators measured more methane than other researchers as well as higher concentrations of propene than 1,3-butadiene. In our earlier work (G. Kraemer PhD thesis, Yale University, 1992), we found that Manganese oxides were effective at converting cyclohexane to smaller hydrocarbon products at temperatures around 1000K. Ethylene was the predominant product observed and methane was next possibly explaining the increased methane production observed by Kralikov et al. Zeppieri et al. measured MCH decomposition in a turbulent flow reactor at slightly higher temperature range than used in the current study (1050-1200K versus 500-1100K). The apparent activation energy was found to be 265kJ/mol indicating significant secondary radical reactions. The order of intermediate products was similar to our studies with the exception of methane which we observed at higher levels. Our apparent activation energy observed varied slightly over the pressure range studied and overall rate was slightly higher than Zeppieri et al. This was not surprising as the rate measured is an overall rate and depends importantly on radical concentrations so the dilution strategy and third body reactions are important.

The intermediate product profiles can be analyzed by examining the fate of the predominant radical formed from MCH decomposition. The subsequent fate of the cyclohexyl radical is ring opening through C-C β-scission and conversion to smaller species. C-H β-scission leading to cyclohexene is a minority reaction channel at our conditions as observed from the species material balances. The reactions of linear C6H11 and C6H12 isomers has been studied previously [60-61]. At the conditions of our study smaller hydrocarbons formed from the linear C6H11 radical are predominantly ethylene from C-C β-scission.and ethylene and 1,3-butadiene from C-H β-scission consistent with the discussion in reference [59]. Propene is the next highest intermediate observed in our study. C_5H_8 (isoprene) is also observed in somewhat smaller quantities and may be used in a test of reaction channel for the initial MCH decomposition. An order of magnitude analysis by Zeppieri et al. [59] suggests that H atom abstraction reactions predominate MCH decomposition. Their analysis from published rate data for H abstractions from alkanes suggests that tertiary H atom abstraction predominates (abstraction of H from the carbon attached to the methyl group). The radical formed can undergo C-H β-scission to form methyl-cyclohexene or more likely according to our species profiles C-C

β-scission to form a C7H13 radical as shown below:

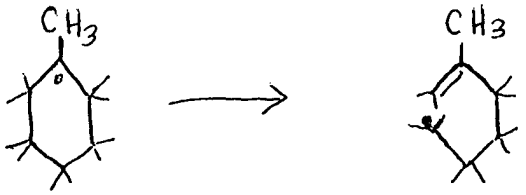

Isoprene can be formed when C-C β-scission occurs followed by C-H β-scission (also yeilds ethylene). A similar sequence with a final C-C β-scission leads to two ethylenes and a propene. The predominace of ethylene as an early reaction intermediate is explained by this reaction path analysis. Our results are in agreement with the analysis of Brezinsky and coworkers [59]. Although some elementary rate measurements have been made on similar systems [57,60,62] not enough experimental information exists to compile a full reaction mechanism without estimating reaction parameters. It will also be key to correctly model radical concentrations. Experimental studies of MCH pyrolysis over a variety of conditions are now complete enough to test proposed detailed models. Oxygen addition at temperatures above that where akyl peroxy radicals are stable does not yeild additional intermediates and reaction profiles are generally similar ([59] and our 1997 ASSERT report). Dehydrogenation products, however, are somewhat more predominant at conditions where significant oxygen is present.

Initial aromatic formation is critical to formation of higher hydrocarbons in the bulk and greatly increases deposit formation, Note from Table #1 (50ms residence time) that toluene was observed at significant concentrations (.10ppm) at 869K as compared to 1090K for benzene and the higher aromatics. Toluene was the only aromatic compound observed in the supercritical fuel studies after significant fuel stressing (24hrs at 675K and in the presence of oxygen). In addition, our work shows that benzene is likely produced by reaction of smaller MCH decomposition products. Benzene is not observed in any of our experiments until the initial fuel decomposition was nearly complete as low as 975K or 1090K at the conditions reported in Table #1. In our fuel stressing experiments (P_R=1.05, T=625K and 24hr residence time) no benzene was observed even though a REMPI technique was used to check the VUV-MS results. This means that if higher hydrocarbon formation in the bulk phase occurred at small amounts in supercritical fuel processing conditions it would most likely be through formation of toluene by either surface reaction, dehydrogenation accelerated by catalytically active surfaces, the presence of alkyl peroxides or surface hot spots.

3.5 Formation of Higher Hydrocarbon Species in the Bulk Phase at T<850K

Because toluene (either formed by surface or bulk phase reactions) is the first and the most prominent aromatic product observed at low temperatures of supercritical fuel application,

we chose to study how second ring products such as naphthalene are formed from toluene as compared to other aromatic hydrocarbons. The fuel in a co-flowing methane/air non-premixed flame was doped with 2500 to 1900 ppm of benzene, toluene, ethylbenzene, styrene, and phenylacetylene. Temperature and species measurements on the centerline in the resulting flames revealed that the additives did not change the overall flame structure, but did increase soot volume fractions and the concentrations of most aromatic hydrocarbons. The H atom and acetylene concentrations in these flames are approximately the same. Thus, if acetylene addition to phenyl type radicals is the major pathway to naphthalene for all dopants, the naphthalene concentration should increase in the same order as the phenyl acetylene. Figures 21 and 22 show the centerline phenyl acetylene and naphthalene concentrations in each flame as a function of height above the burner. Note that although the ethyl benzene and toluene additives produce about equivalent phenyl acetylene concentrations (lower than for the other additive with the exception of benzene) they produce among the highest naphthalene concentrations. Naphthalene production from toluene and ethyl benzene also peaks at a somewhat lower height than for the other additives with the exception of phenyl acetylene (which because it was a fuel additive was at the highest concentration low in the flame). Figure 21 shows the maximum centerline phenyl acetylene plotted against the maximum centerline naphthalene for each aromatic fuel. In the un-doped flame, the benzene-doped flame and the styrene doped flame, the naphthalene concentration scales with the phenyl acetylene concentration as shown by the straight line through the origin that passes through these three data points. The naphthalene concentrations form the toluene and ethyl-benzene doped flames however, are not consistent with formation primarily through sequential acetylene additions. These flames have essentially the same phenyl acetylene and acetylene concentrations at all heights as the benzene doped flame yet twice the maximum naphthalene concentration. In addition, these flames have half the maximum phenyl acetylene concentration as the styrene-doped flame but more naphthalene. These observations indicate that another channel for naphthalene production must exist for the toluene and ethyl benzene additives.

The decomposition pathways for these two additives at moderate temperatures produces benzyl radicals. Colket and Seery [64] studied toluene pyrolysis in a shock tube reactor and found anomalously high naphthalene concentrations. They proposed the following overall reaction to explain the high naphthalene concentrations observed:

$$C_6H_6\text{-}CH_2\cdot + C_3H_3 = C_{10}H_8 + 2H$$

Although this reaction has not been studies experimentally or theoretically C3 products are prominent MCH decomposition products so that this type of pathway might be important in supercritical fuel systems.

Analysis of the data from this work lead to the following conclusions:

1) The H-abstraction/C2H2-addition mechanism is responsible for the naphthalene formed in the undoped, benzene-, styrene-, and penylacetylene-doped flames.

2) A second source of naphthalene, involving benzyl radicals, was important in the toluene- and ethylbenzene-doped flames. A promising candidate for this pathway is the reaction between benzyl and propargyl radical suggested by Colket and Seery (1994).

3) The maximum soot volume fractions and naphthalene concentrations increase among the flames in the same order, indicating that naphthalene is the critical soot formation step for fuel mixtures containing one-ring compounds.

4) Soot formation models that base inception rates on benzene or acetylene concentrations are not appropriate for soot and higher hydrocarbon production during decomposition of advanced fuel mixtures. Additional routes for naphthalene and larger PAH are accessible which were not evaluated by current model correlations. Soot in these studies does not scale with acetylene concentration, or single ring dopant concentration because the naphthalene formed is a function of the structure of the single ring dopant.

Overall Conclusions

Methods for measuring speed of sound and heat transfer coefficients in supercritical reacting fluids were developed and tested. These measurements were used to show that relationships for predicting supercritical fuel properties near the critical point are not valid and that in-situ measurement is important. Measurement of reaction products from the thermal stressing of MCH over a wide range of pressures and temperatures with and without oxygen contamination shows that 1) dissolved oxygen is important in the formation of products in the bulk phase 2) insoluble residues from hydrocarbons at temperatures less than 850K are likely caused by the presence of oxygen and/or an active surface 3) the only aromatic species observed at low temperatures was toluene and naphthalene production can proceed through reactions of the benzyl radical 4) the coating of the wall of the supercritical fuel reactor with catalytically inactive titanium nitride prevented significant surface activity. Deoxygenation and passivation of metallic surfaces can be used in actual aircraft systems to reduce deposit formation. Prevention of hot-spots is also critical as rupture of the MCH ring can quickly produce benzene and higher mass aromatics.

References

1. Kim, S. and K. P. Johnston, Ind. Eng. Chem. Res. 26, 1206 (1987).
2. Yonker, C. R. and R. D. Smith, J. Phys. Chem. 92, 235 (1988).
3. Nakagawa, K., A. Ejiri, K. Kimura, and M. Nishikawa, Phys. Scripta 41, 140 (1990)
4. Nakagawa, K., Radiat. Phys. Chem. 37, 5/6, 643 (1991)
5. Brennecke, J. F., D. L. Tomasko, J. Peshkin and C. A. Eckert, Ind. Eng. Chem. Res. 29, 1682 (1990).
6. Sun, Y.-P., M.A. Fox, and K.P. Johnston, J. Am. Chem. Soc. 114, 1187 (1992)
7. Carlier, C. and T. W. Randolph, AIChE J. 39, No.5 (1993)
8. Cochran, H.D., and L.L. Lee, ACS Symp. Ser. 448, 60 (1992)
9. Debenedetti, P. G., Chem.Eng. Sci. 42, 2203 (1987).
10. Knutson, B. L, D. L. Tomasko, C. A. Eckert, P. G. Debenedetti and A. A. Chialvo, Supercritical Fluid Technology, Bright F. V. and M. E. P. McNally, Eds., ACS Symp. Ser. 448, 60 (1992).
11. Johnston, K. P. and C. Haynes, AIChE J. 33, 2017 (1987).
12. Chateauneuf, J. E., C. B. Roberts, and J. F. Brennecke, Supercritical Fluid Technology, Bright F. V. and M. E. P. McNally, Eds., ACS Symp. Ser., 448, 48 (1992)
13. Zagrobelny, J and F. V. Bright, J. Am. Chem. Soc 114, 7821-7826 (1992).
14. Roberts, C. B., Z. Zhang, J. F. Brennecke, and J. E. Chateauneuf, J. Phys. Chem. 97, (1993)
15. Otto, B., J. Schroeder and J. Troe, J. Chem. Phys. 81, 202-213 (1984).
16. Combes, J. R., K. P. Johnston, K. E. O'Shea and M. A. Fox, Supercritical Fluid Technology, Bright F. V. and M. E. P. McNally, Eds., ACS Symp. Ser. 448, 31 (1992).
17. Molin, Y.N., K.M. Salikhov, and K.I. Zamaraev, Spin Exchange Principles and Applications in Chemistry and Biology, Springer Verlag, New York (1980)
18. Randolph, T. W. and C. Carlier, J. Phys. Chem 96, 5146-5151 (1992).
19. O'Brien, J. A., T. W. Randolph, C. Carlier and S. Ganapathy, AIChE J. 39, 6 (1993)
20. Prausnitz, J. M., Molecular Thermodynamics of Fluid Phase Equilibria, Prentice-Hall, Englewood Cliffs, New Jersey, p. 107 (1969).
21. Ganapathy, S., O'Brien, J.A., and Randolph, T.W., "Effect of Solute-Solute Correlations on Rapid Reactions in Supercritical Fluids," *AIChE J.*, 11(2), 346-356, 1995.
22. Allen, M. P. and D. J. Tildesley, Computer Simulation of Liquids, Oxford University Press, New York (1987)
23. Smit, B., P. De Smedt and D. Frenkel, Mol. Phys. 68, 931 (1989).
24. McGuigan, D.B. and P.A. Monson, Fluid Phase Equilibria 57, 227 (1990).
25. Hirschfelder, J. O., C. F. Curtiss and R. B. Bird, Molecular Theory of Gases and Liquids, Wiley, New York (1954).
26. Chapman, S., and T.G. Cowling, The Mathematical Theory of Non-Uniform Gases, Cambridge University Press, Cambridge U.K. (1970)
27. Randolph, T.W., J.A. O'Brien, and S. Ganapathy, J. Phys. Chem., In Press 1994
28. Smoluchowski, M. V. Z., Physikal Chem. 92, 129 (1917).
29. Bartels, D.M., A.D. Trifuac and R.G. Lawler, Chem. Phys. Lett. 152, 109-115 (1988).
30. Bunker, D.L., J. Chem. Phys. 32, 1001-1005 (1960)
31. Agmon, N., J. Chem. Phys. 81, 3644-3647 (1984)
32. Chandrasekhar, S., Rev. Mod. Phys. 15, 1-89 (1943)
33. Szabo, A., K. Schulten, and Z. Schulten, J. Chem. Phys. 72, 4350-4357 (1980)
34. Zawadzki, A.G. and J.T. Hynes, J. Phys. Chem. 93, 7031-7036 (1989).
35. Edwards, USAF Supercritical Hydrocarbon Fuel Interests, AIAA paper 93-0807, AIAA, Washington D.C., January (1993).
36. Chin and A.H. Lefebvre, Experimental Techniques for the Assessment of Fuel Thermal Stability, J. Propulsion, 8 (6) (1992) 1152.

37. Lander, and A.C. Nixon, Endothermic Fuels for Hypersonic Vehicles, Journal of Aircraft, 8(4) (1971) 200.
38. Dickinson and C.P. Welch, Heat Transfer to Supercritical Water, Trans. ASME., 80, (1958) 746.
39. W.F. Hines and H. Wolf, Pressure oscillations associated with heat transfer to hydrocarbon fluids at supercritical pressures and temperatures, ARS Journal, March, (1962) 361.
40. Faith, G.H. Ackerman, and H.T. Henderson, Heat Sink Capabilities of Jet-A Fuel: Heat Transfer and Coking Studies, NASA CR-72951, NASA Lewis Research Center, Cleveland, OH, July 1971.
41. Papaionnou, D. Ziakas, and C. Panayiotou, Volumetric Properties of Binary Mixtures, J. Chem. Eng. Data, 36 (1991) 35.
42. Schneider, Ultrasonic absorption in the critical temperature region J. Chem. Phys 18 (1950) 1300.
43. Schneider, Sound velocity and sound absorption in the critical temperature region Can J. Chem. 29, (1951) 243.
44. Herget, Ultrasonic velocity in carbon dioxide and ethylene in the critical region J. Chem. Phys. 8 (1940) 537.
45. Belinskii, V.F. Nozdrev, and T. Nuriddinov, Acoustic properties of sulfur hexafluoride in the postcritical region, Russ. J. Phys. Chem., 47 (1973) 811.
46. Belinskii, V.F. Nozdrev, and T. Nuriddinov, Acoustical properties of sulfur hexafluoride in the critical region Sov. Phys. Acoust., 19 (1974) 577.
47. Thoen, and C.W. Garland, Sound Absorption and dispersion as a function of density near the critical point of xenon, Phys. Rev. A, 10 (1974) 1311.
48. Colgate, A. Sivaraman, C. Dejsupa, and K.C. McGill, Acoustic cavity method for phase boundary determinations: The critical temperature of CO2 Rev. Sci. Instrum. 62 (1991) 198.
49. Colgate, A. Sivaraman, and C. Dejsupa, Sonic speed and critical point measurements in ethane by the acoustic resonance method Fluid Phase Equil. 76 (1992) 175.
50. V.K Popov, J.K. Banister, V.N. Bagratashvili, S.M. Howdle, and M. Poliakoff, Acoustic and Photoacoustic Measurements in Supercritical Fluids; A New Approach to Determining the Critical Point of Mixtures, J. Supercritical Fluids, 7 (1994) 69.
51. Kordikowski, D.G. Robertson, A.L. Aguiar-Ricardo, V.K. Popov, S.M. Howdle, and M. Poliakoff, Probing Vapor/Liquid Equilibria of Near-Critical Binary Gas Mixtures by Acoustic Measurements, J. Phys. Chem., 100, (1996) 9522.
52. Younglove and J.F. Ely, Thermophysical Properties of Fluids, J. Phys. Chem. Ref. Data, 16(4) (1987) 577.
53. Reid, J.M. Prausnitz, and B.E. Poling, The Properties of Gases and Liquids, 4th Ed., McGraw-Hill, USA 1987.
54. Rowlinson, and F.L Swinton, F.L., Liquids and Liquid Mixtures, 3rd Ed., Butterworth, Great Britain 1982.
55, Boyle, J., and Pfefferle, L., Combust. Sci. and Tech., 70:18887-203(1990)
56. Miljovska, J., Ph.D. thesis, Department of Chemical Engineering, Yale University, New Haven, 1995.
57. Brown, T. and King, K.D., Int. J. of Chem. Kinet., 21, 251(1989)
58. Zeppieri, S., Brezinsky, K., and Glassman, I., Comb. and Flame, 108:266-286(1997)
59. Kralikova, U., Bajus, M., and Baxa, J., Collect. Czech. Chem. Commun., 52:1527-1544(1987)
60. Kalinenko, R.A., Shevelkova, L.V. etc., Ndftekhimija, 16, 100)1976)
61. Tsang, W., Int. J. Chem. Kinet., 1119(1978)
62. Simmie, J.M., Int. J. Chem. Kinet., 227(1978)
63. Korzun, N.V., Magaril, R.Z. etc., Russ. J. Phys. Chem., 53, 631(1979)
64. Colket, M. B. and Seery, D., 25th Symposium Intl' on Combustion, Combustion Institute, Pitts., PA, 1994, P. 883.

Figure Captions

Figure 1: Local to bulk density ratio vs. r* calculated from the modified partial fluctuation integral and the OZPY integral equation.

Figure 2: The effect of collision length-scale r* (non-dimensionalized in solute L-J units) on the normalized solvent-solute collision rate constant. The line is $g_{12}(r)$ obtained from the same simulation runs, while the closed circles represent the rate constants. There is exact quantitative agreement for all three densities shown.

Figure 3: Comparison of the effect of collision length-scale r* on the solute-solute collision rate constants and reaction rate constants. All of the rate constants have been normalized by the modified kinetic theory result. Also shown in dotted lines is the Smoluchowski limit. The open circles represent the collision rate constants and the closed circles represent the reaction rate constants. The full line shown represents the modified kinetic theory prediction. These comparisons are shown over three different densities.

Figure 4: Comparison of the reaction rate constants from BD simulations and EPR studies as a function of 1/density. The BD results are for a collision radius of $r=1.0\sigma_{22}$. The horizontal line represents the kinetic theory result while the skewed line corresponds to the Smoluchowski prediction. EPR results have been scaled by a factor of two; this factor is the lower bound on probability effects on the Heisenberg spin-exchange reaction.

Figure 5: A plot of the collision lifetime distributions over the reduced density range of 0.1455 to 1.455. The ordinate represents the frequency of the collision lifetimes, while the abscissa denotes the collision lifetime (in solute L-J units). All distributions are plotted on the same scale. These lifetimes were estimated for a collision radius of $r=1.57\sigma_{22}$ Interestingly, most of the density space where the lifetime distributions are distinctly bi-modal falls in the near- and supercritical region for this collision length-scale.

Figure 6. Block diagram of circuit used to measure the velocity of sound.

Figure 7a. Cross-section of the feedthrough assembly.

Figure 7b. Cross-section of the reactor head with feedthrough and quartz crystal. a - Inlet, 1/4" HiP to 1/8î" NPT, b - Position of feedthrough, c - Vented, silver coated stainless steel O-ring, d - Stainless steel bushing, e - Pressure spacer, f - Threaded nut, g - Spacer ring, h - X-cut quartz crystal: 250 kHz, i - Stainless steel ring grounding one face of crystal to the vessel, j - Threads on the head, k - Ceramic holder

Figure 8. Velocity of sound in methylcyclohexane at 274K. Calculated values are from a modified BWR equation of state for pentane combined with a corresponding states approach.

Figure 9. Velocity of sound in methylcyclohexane in the vicinity of the critical point.

Figure 10. T_c, P_c for different MCH-benzene mixtures. All mixture compositions in mole percent. Mixture critical parameters are evaluated using method 1- pseudocritical method with simple mixing rules and method 2- binary interaction parameters, second virial coefficients.

Figure 11. Heat transfer coefficient for natural convection in n-heptane by hot wire anemometry. Continuous line represents correlation; squares are experimentally determined values.

Figure 12. Methylcyclohexane pyrolysis at 760torr and 150ms residence time: major products

Figure 13. Methylcyclohexane pyrolysis at 760torr and 150ms residence time: mass 40 -68 products

Figure 14. Methylcyclohexane pyrolysis at 760torr and 150ms residence time: Higher hydrocarbon products

Figure 15. Methylcyclohexane pyrolysis at 760torr and 50ms residence time: major products

Figure 16. Methylcyclohexane pyrolysis at 760torr and 50ms residence time: mass 40 -68 products

Figure 17. Methylcyclohexane pyrolysis at 760torr and 50ms residence time: Higher hydrocarbon products

Figure 18. Methylcyclohexane pyrolysis at 1400torr and 50ms residence time: major products

Figure 19. Methylcyclohexane pyrolysis at 1400torr and 50ms residence time: mass 40 -68 products

Figure 20. Methylcyclohexane pyrolysis at 1400torr and 50ms residence time: Higher hydrocarbon products

Figure 21 Centerline phenyl acetylene concentration, ppm, at the centerline as a function of height above the burner for an aromatic doped methane diffusion flame.

Figure 22 Centerline naphthalene concentration, ppm, at the centerline as a function of height above the burner for an aromatic doped methane diffusion flame.

Figure 23 Maximum naphthalene concentration versus maximum phenyl acetylene concentration for an aromatic doped methane diffusion flame.

Figure 1: Local to bulk density ratio vs. r* calculated from the modified partial fluctuation integral and the OZPY integral equation.

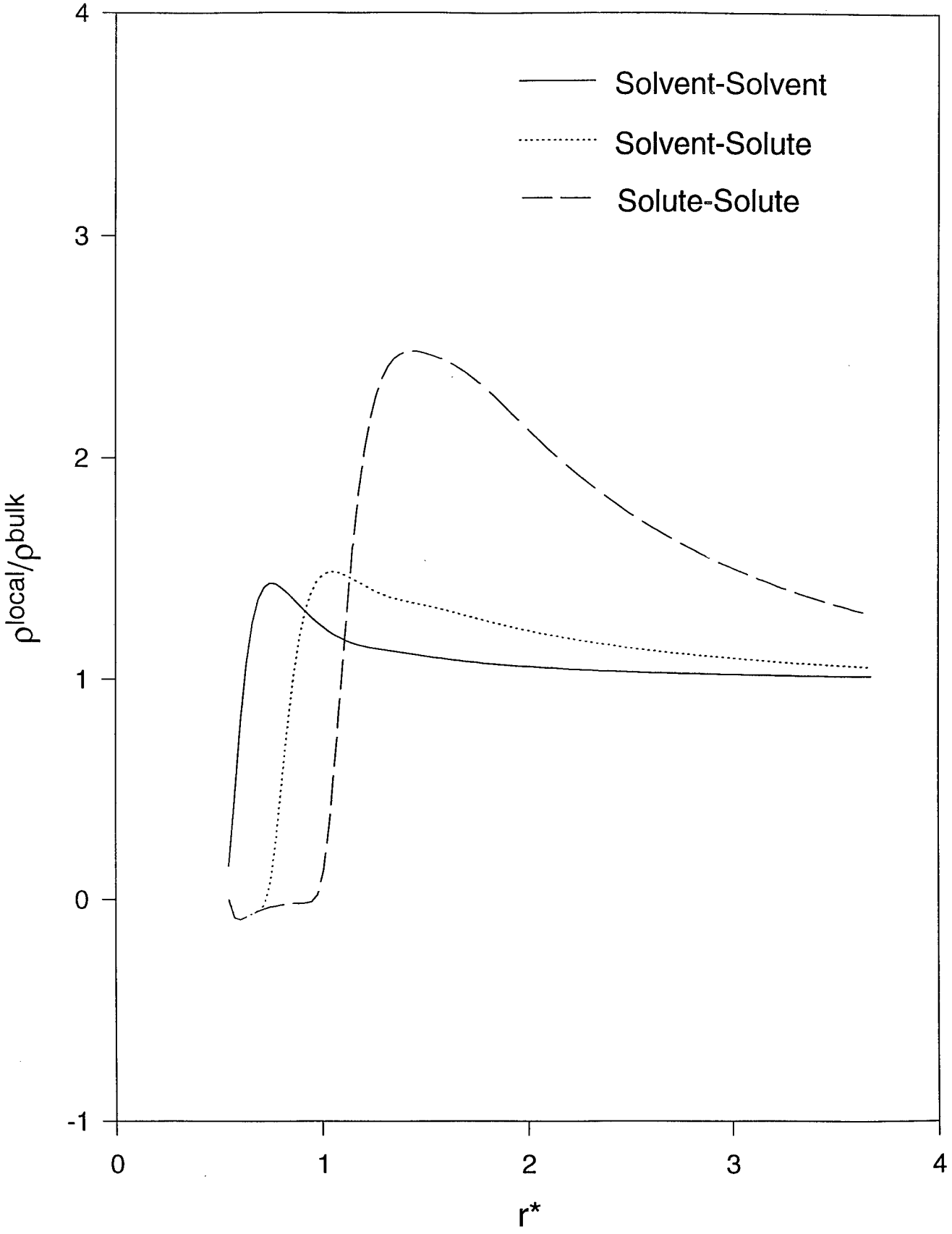

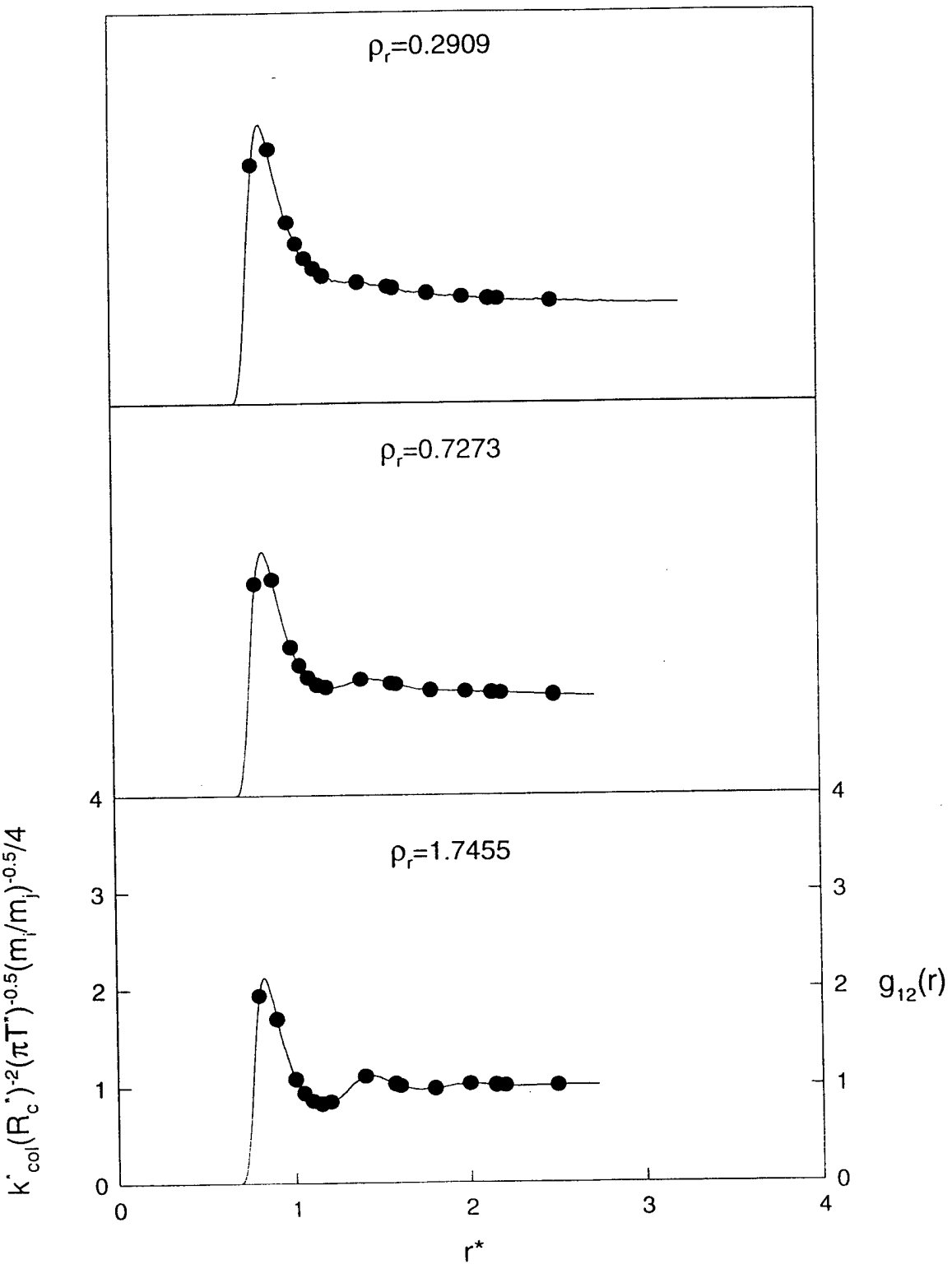

Figure 2: The effect of collision length-scale r* (non-dimensionalized in solute L-J units) on the normalized solvent-solute collision rate constant. The line is $g_{12}(r)$ obtained from the same simulation runs, while the closed circles represent the rate constants. There is exact quantitative agreement for all three densities shown.

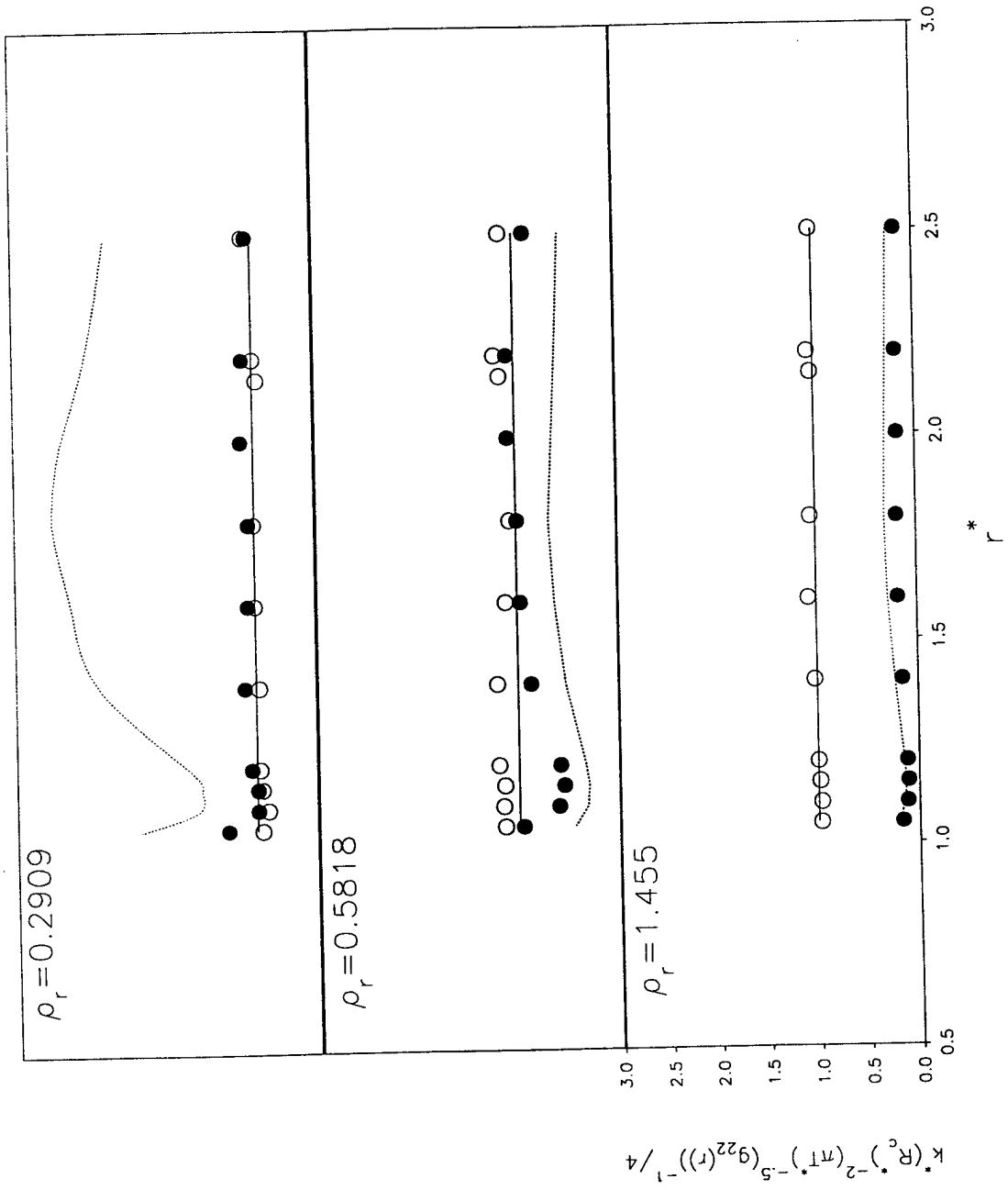

Figure 3: Comparison of the effect of collision length-scale r* on the solute-solute collision rate constants and reaction rate constants. All of the rate constants have been normalized by the modified kinetic theory result. Also shown in dotted lines is the Smoluchowski limit. The open circles represent the collision rate constants and the closed circles represent the reaction rate constants. The full line shown represents the modified kinetic theory prediction. These comparisons are shown over three different densities.

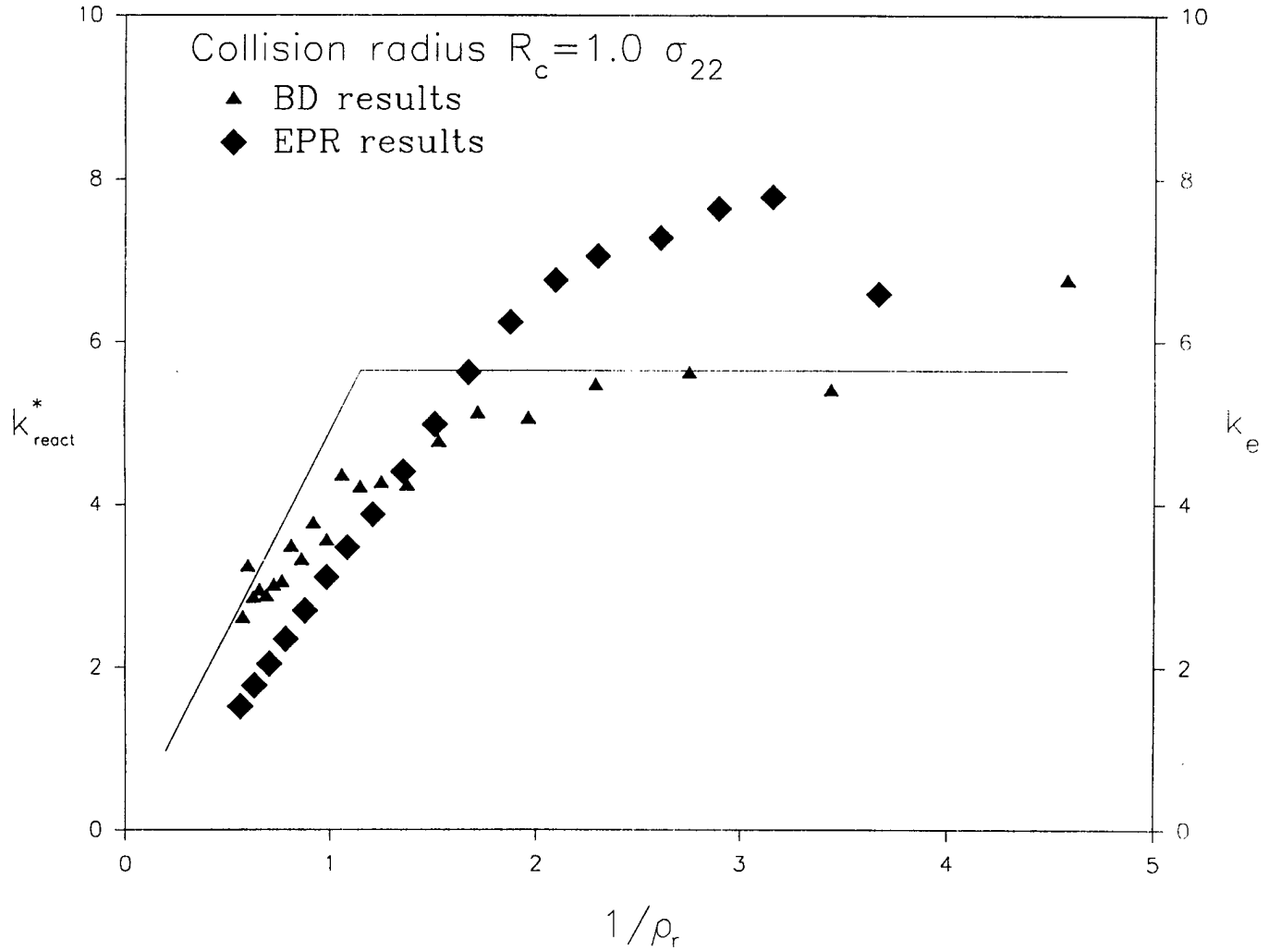

Figure 4: Comparison of the reaction rate constants from BD simulations and EPR studies as a function of 1/density. The BD results are for a collision radius of r=1.0s_{22}. The horizontal line represents the kinetic theory result while the skewed line corresponds to the Smoluchowski prediction. EPR results have been scaled by a factor of two; this factor is the lower bound on probability effects on the Heisenberg spin-exchange reaction.

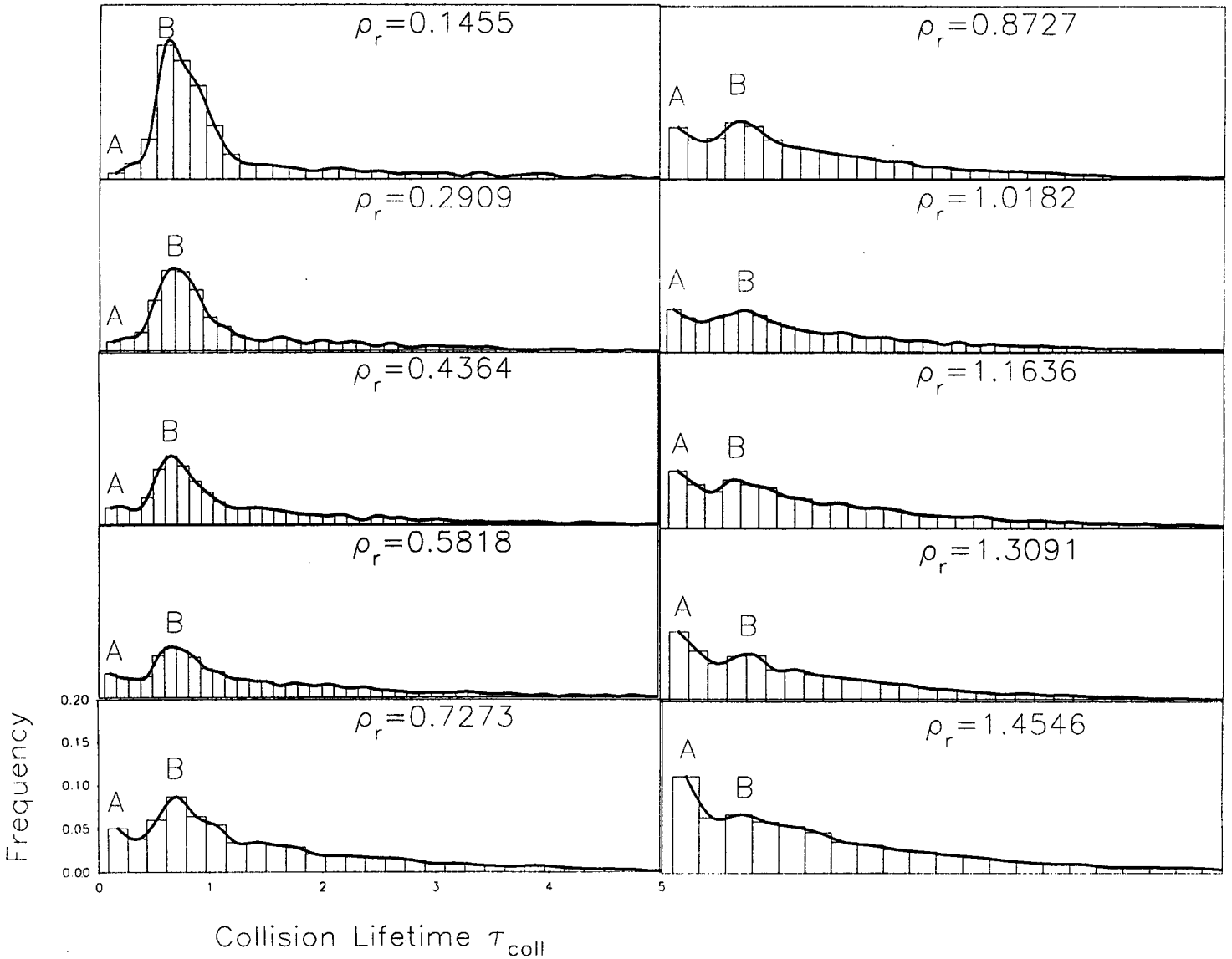

Figure 5: A plot of the collision lifetime distributions over the reduced density range of 0.1455 to 1.455. The ordinate represents the frequency of the collision lifetimes, while the abscissa denotes the collision lifetime (in solute L-J units). All distributions are plotted on the same scale. These lifetimes were estimated for a collision radius of $r=1.57\sigma_{22}$ Interestingly, most of the density space where the lifetime distributions are distinctly bi-modal falls in the near- and supercritical region for this collision length-scale.

Figure 6. Block diagram of circuit used to measure the velocity of sound.

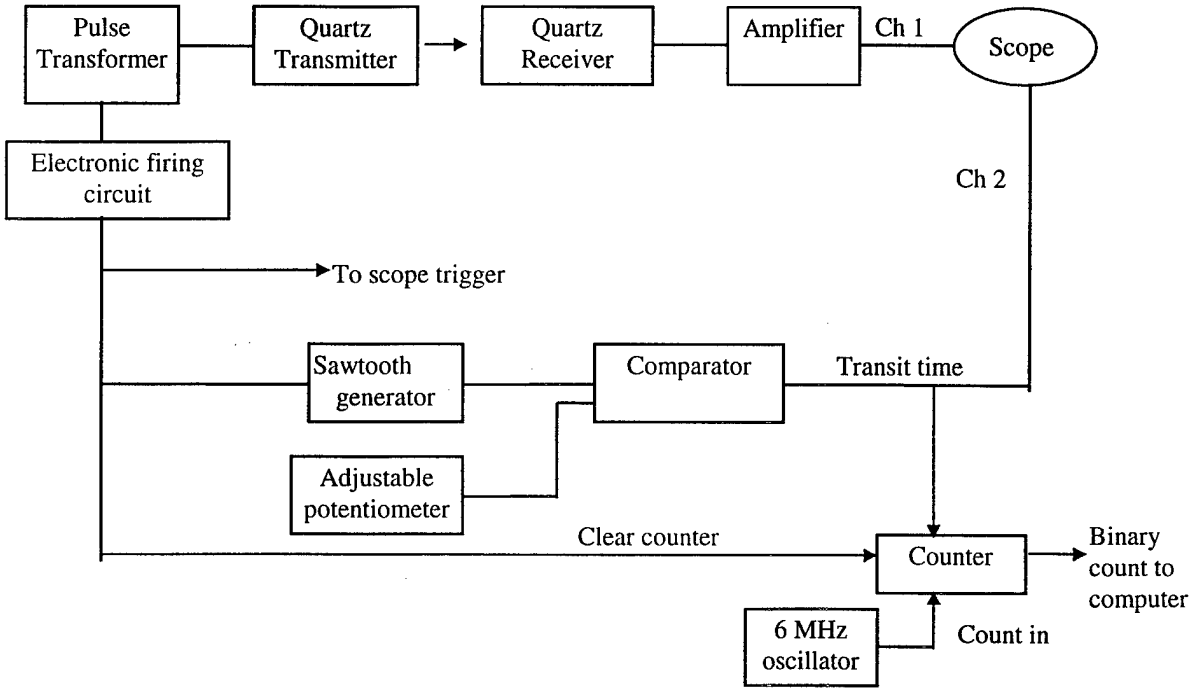

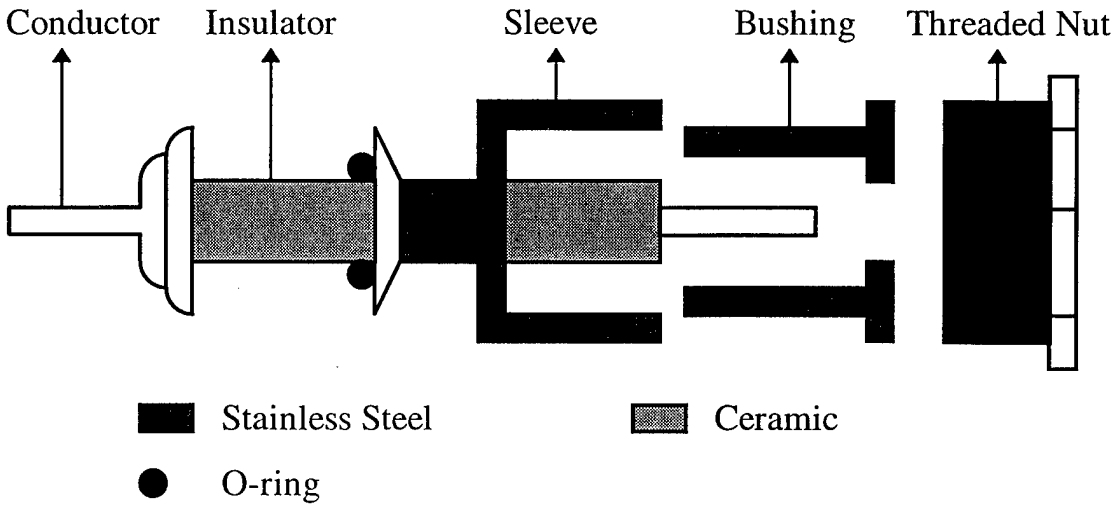

Figure 7a. Cross-section of the feedthrough assembly.

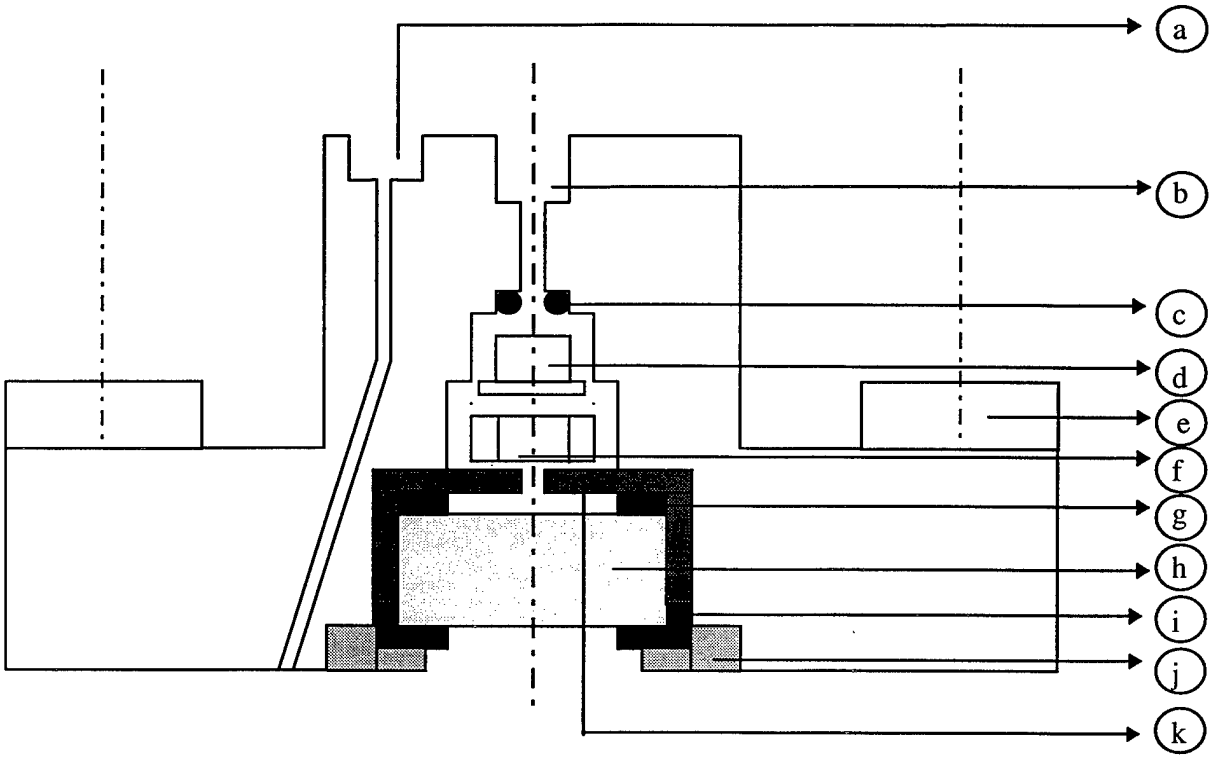

Figure 7b. Cross-section of the reactor head with feedthrough and quartz crystal. a - Inlet, 1/4" HiP to 1/8î" NPT, b - Position of feedthrough, c - Vented, silver coated stainless steel O-ring, d - Stainless steel bushing, e - Pressure spacer, f - Threaded nut, g - Spacer ring, h - X-cut quartz crystal: 250 kHz, i - Stainless steel ring grounding one face of crystal to the vessel, j - Threads on the head, k - Ceramic holder

Figure 8. Velocity of sound in methylcyclohexane at 274K. Calculated values are from a modified BWR equation of state for pentane combined with a corresponding states approach.

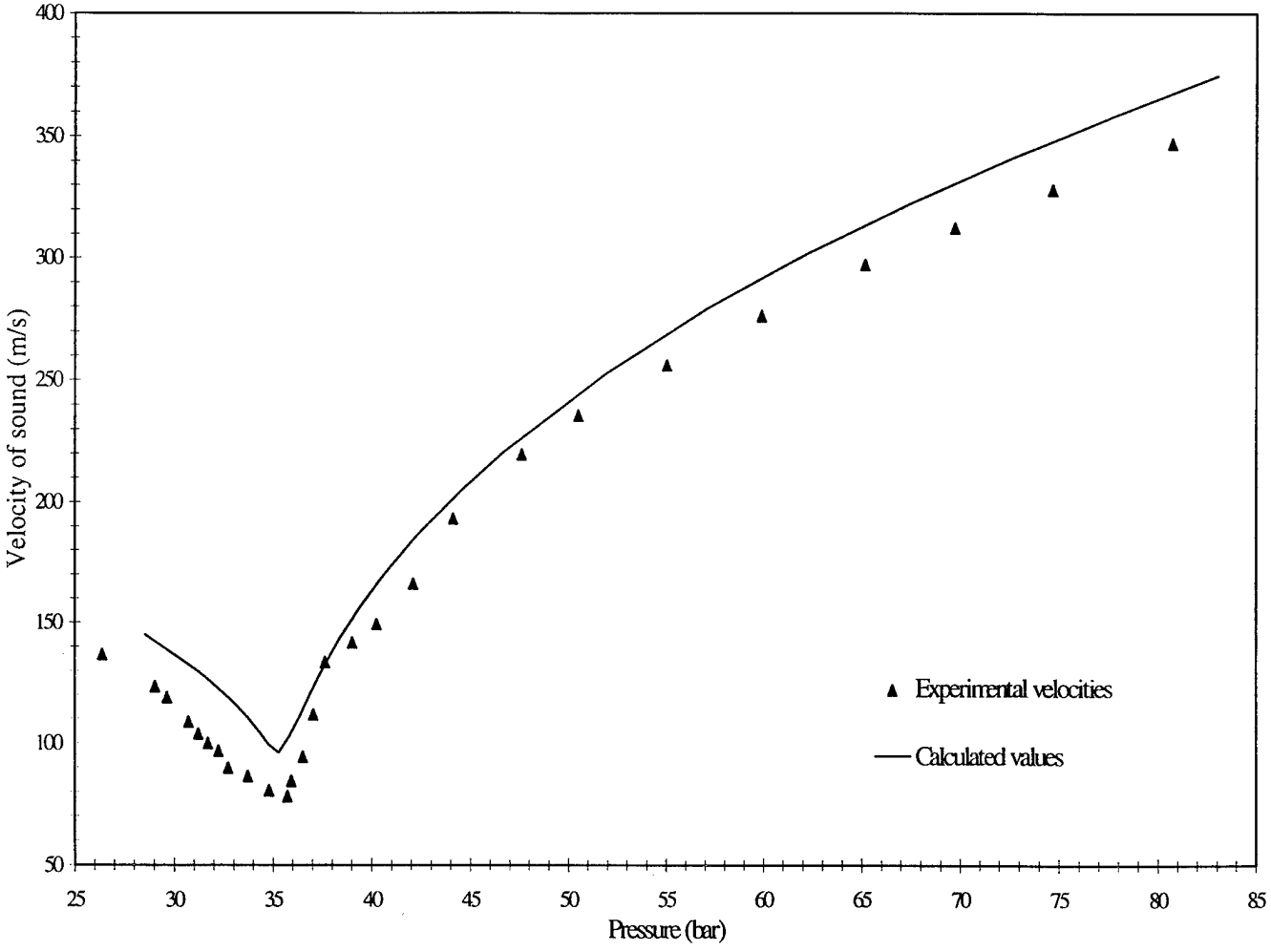

Figure 9. Velocity of sound in methylcyclohexane in the vicinity of the critical point.

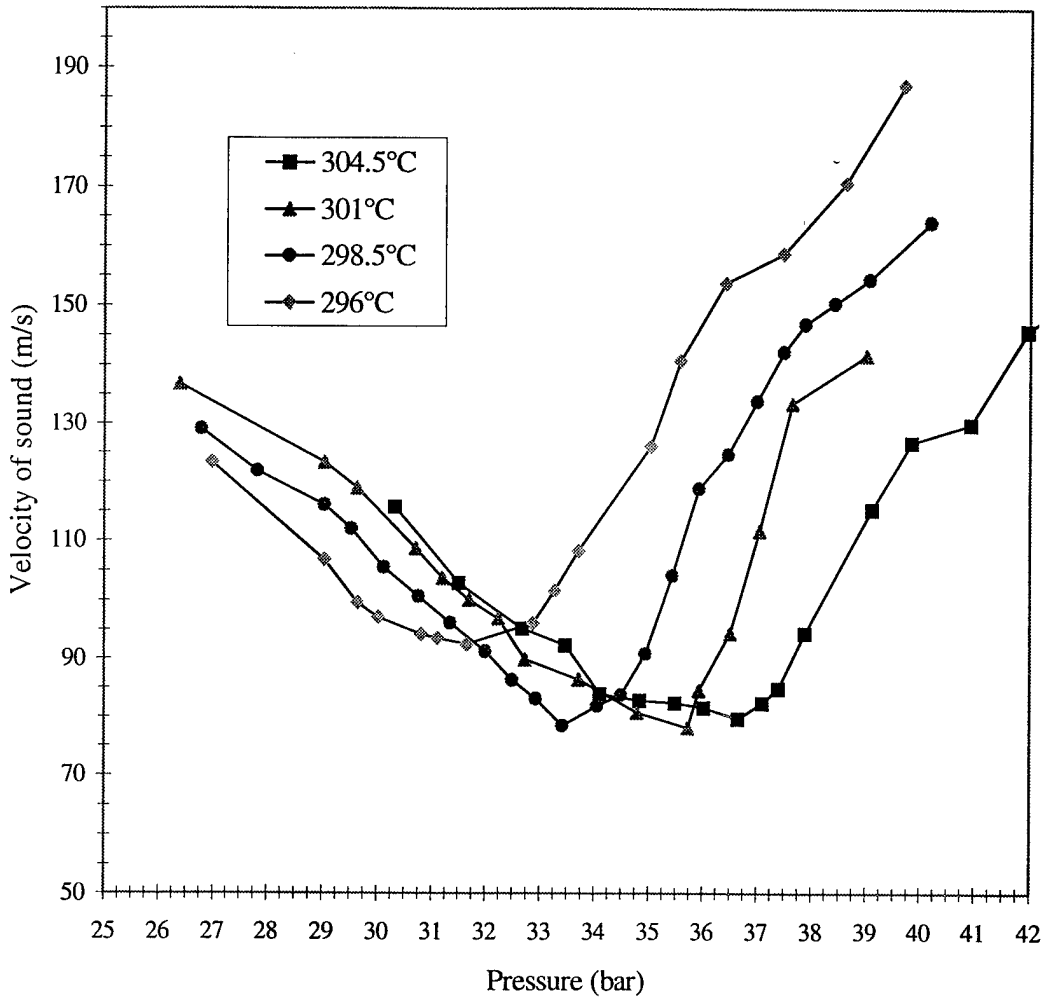

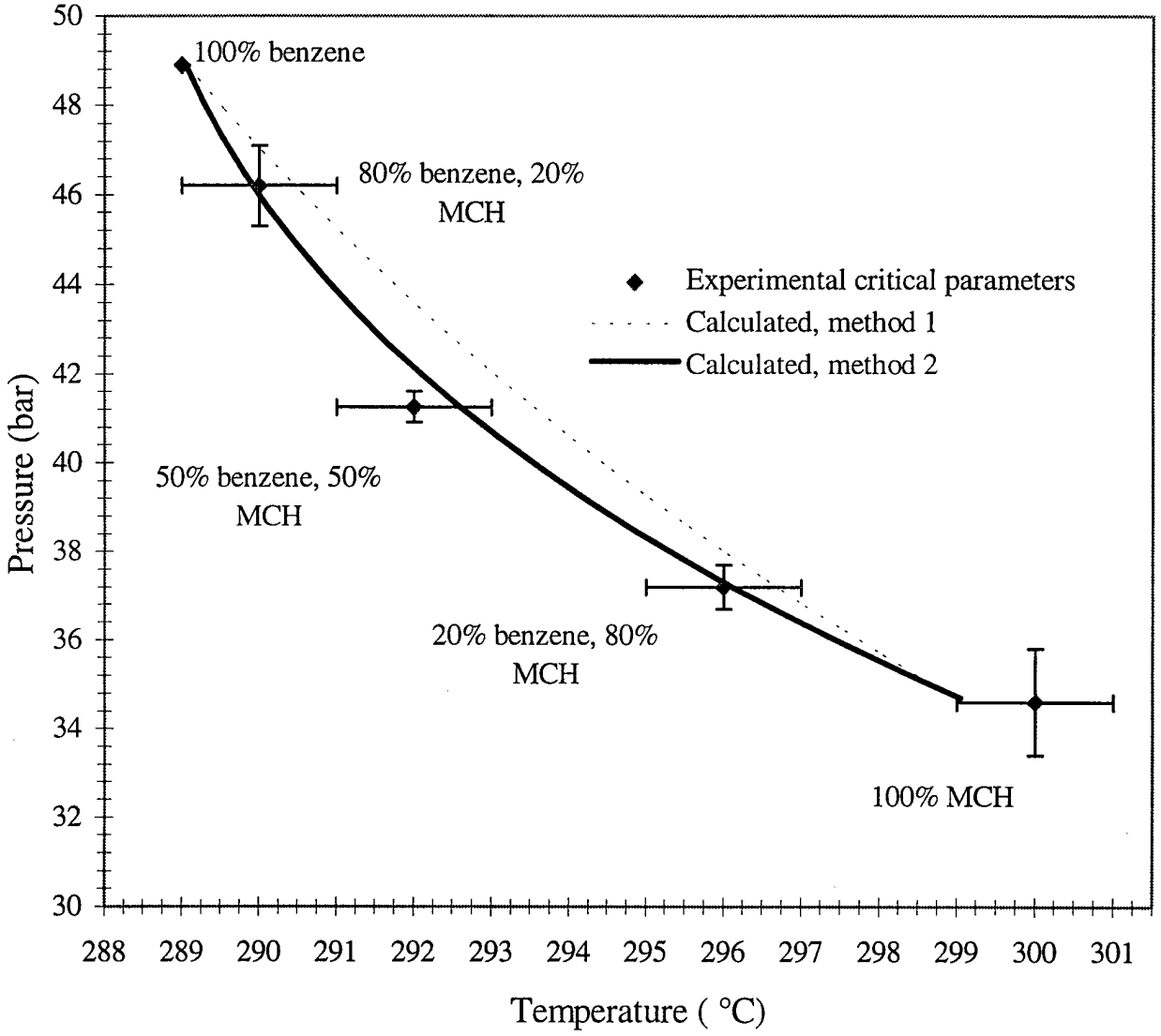

Figure 10. T_c, P_c for different MCH-benzene mixtures. All mixture compositions in mole percent. Mixture critical parameters are evaluated using method 1- pseudocritical method with simple mixing rules and method 2- binary interaction parameters, second virial coefficients.

Figure 11. Heat transfer coefficient for natural convection in n-heptane by hot wire anemometry. Continuous line represents correlation; squares are experimentally determined values.

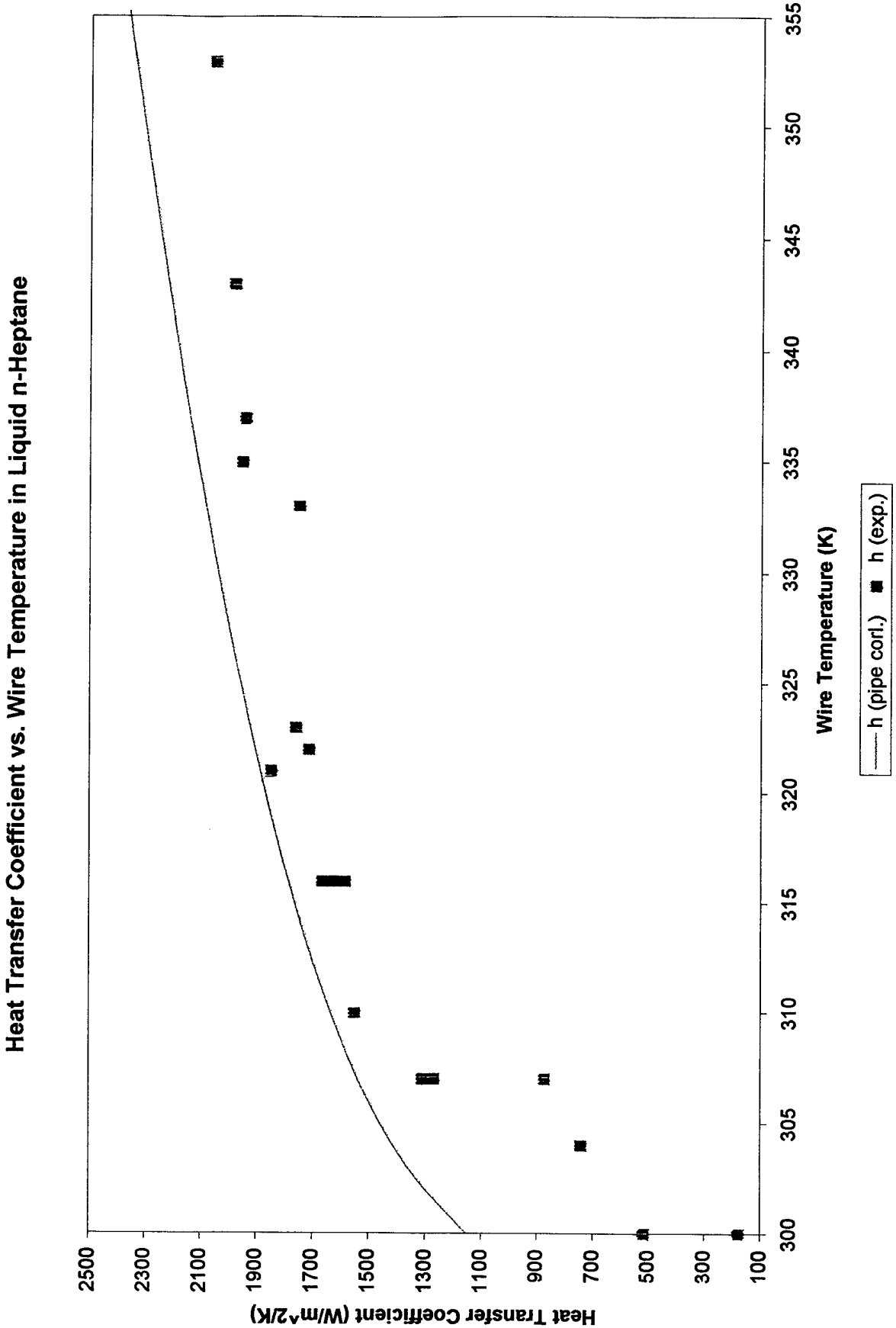

Figure12 MCH pyrolysis, P=760, τ =150ms

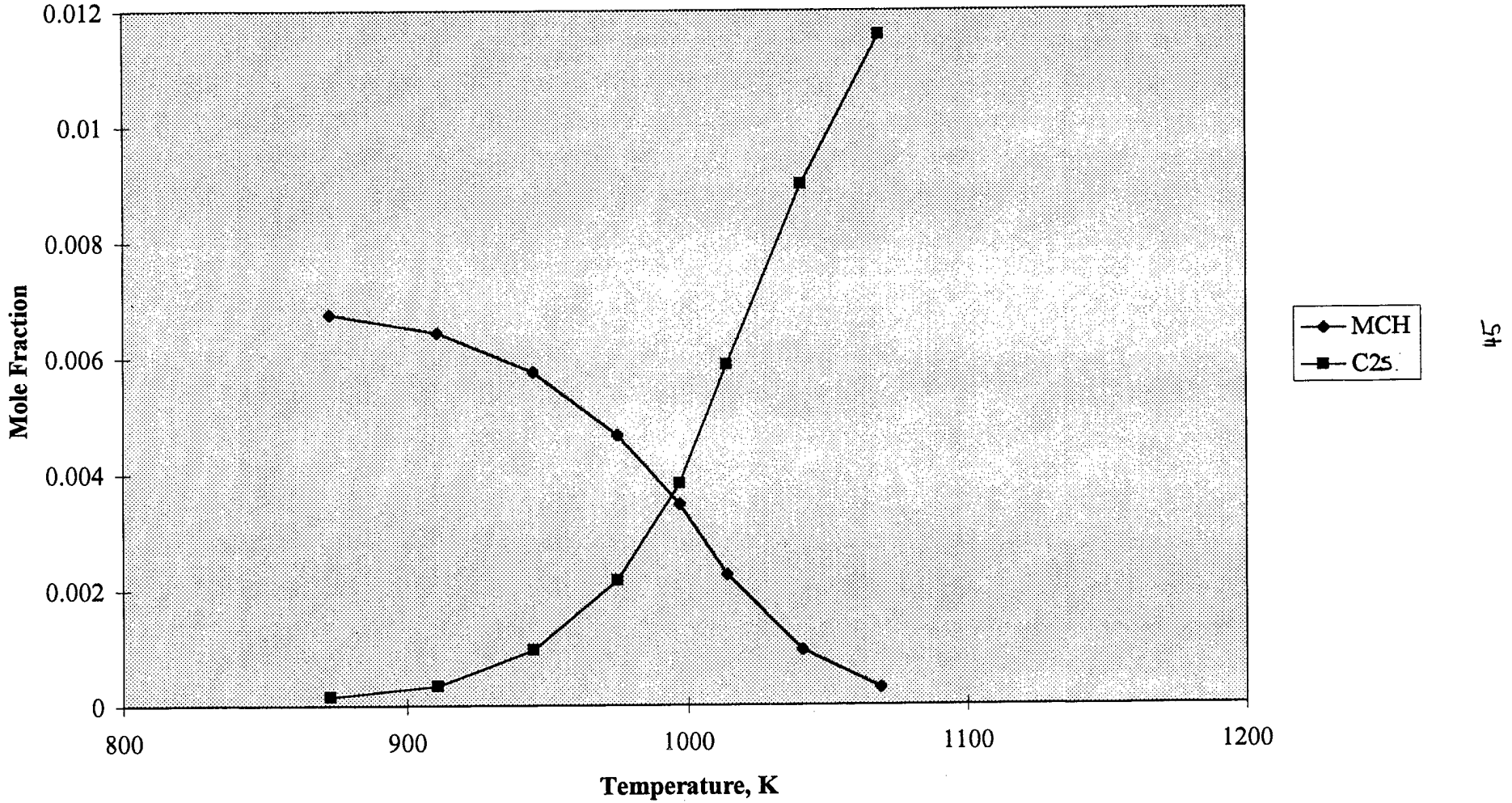

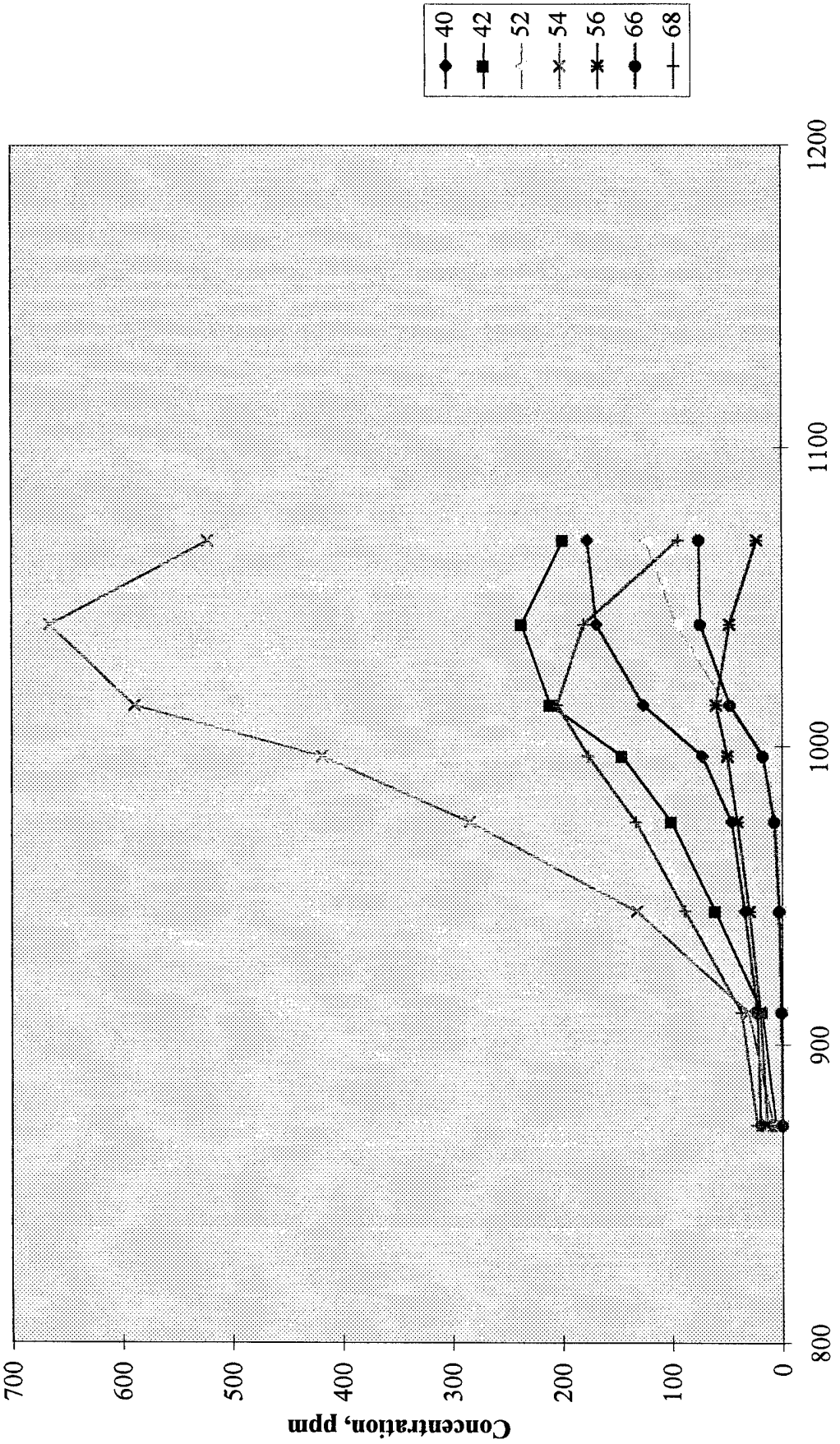

Figure3: Mass 40-68 hydrocarbons formed during MCH pyrolysis, P=760, τ =150ms

Figure 14: Higher hydrocarbons formed during MCH pyrolysis, P=760, τ =150ms

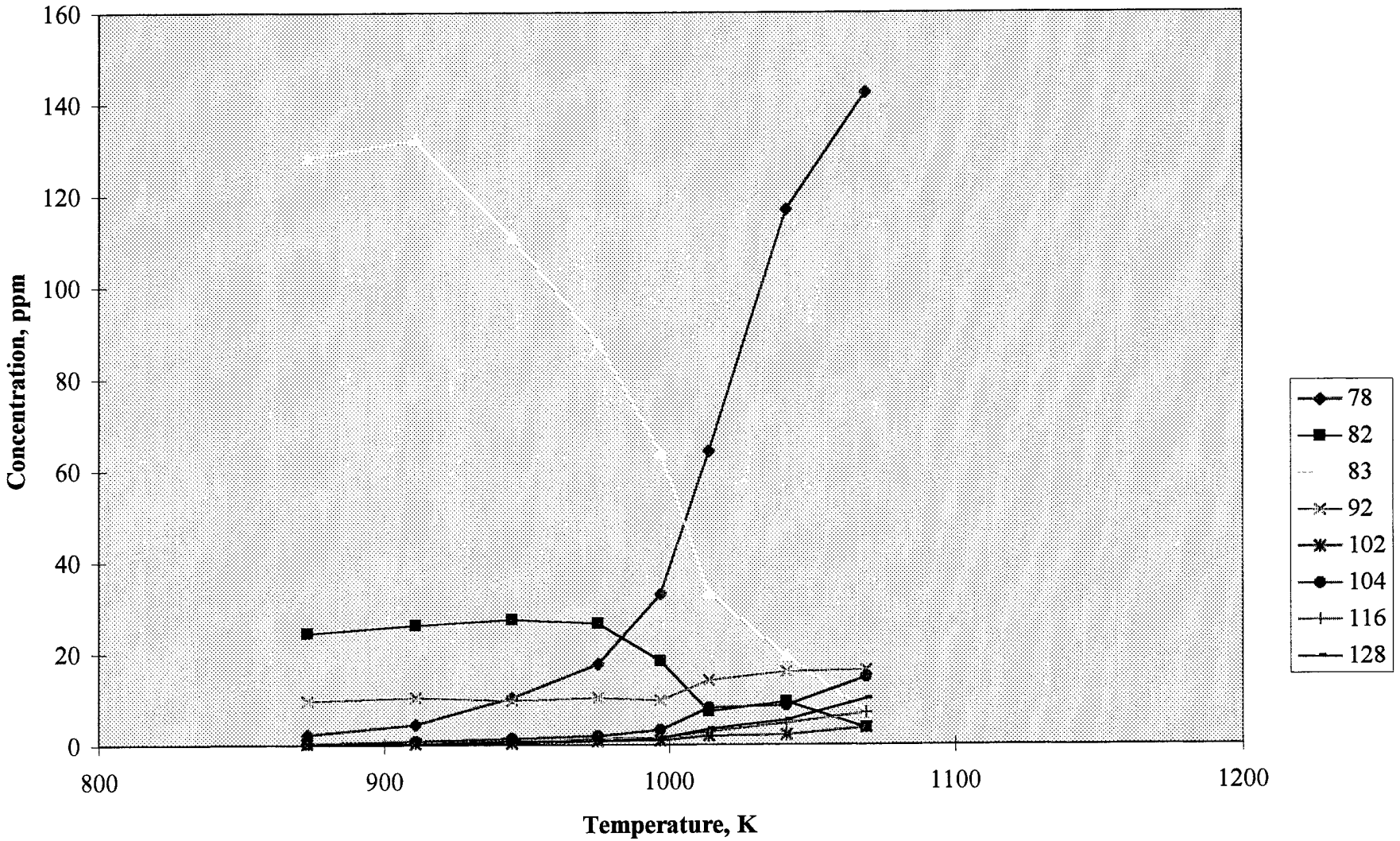

Figure15: MCH pyrolysis, P=760 torr, τ =50ms

Figure 16: Mass 40-68 hydrocarbons formed during MCH pyrolysis, P=760 torr, τ =50ms

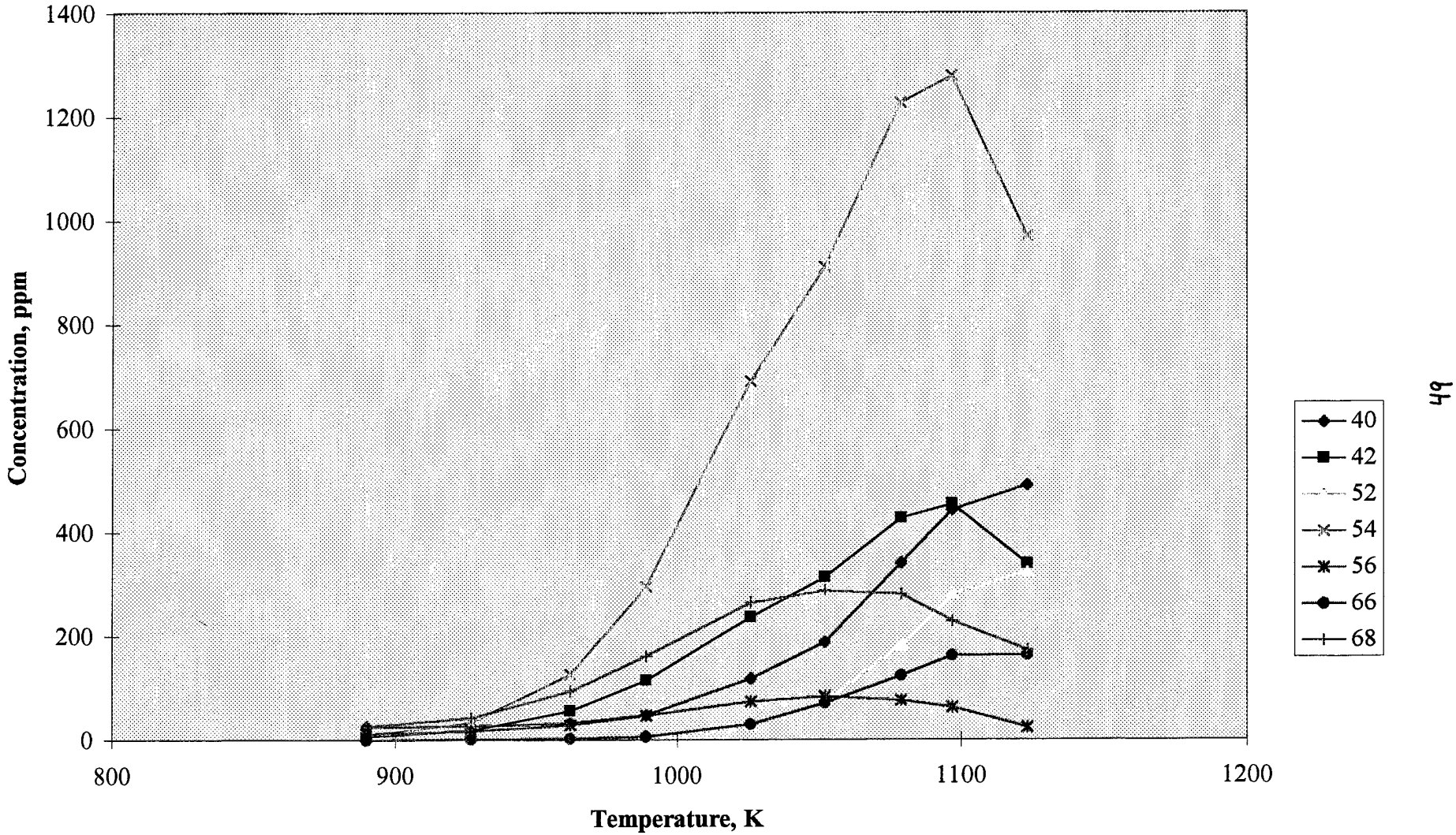

Figure 17. Higher hydrocarbons formed during MCH pyrolysis, P=760 torr, τ =50ms

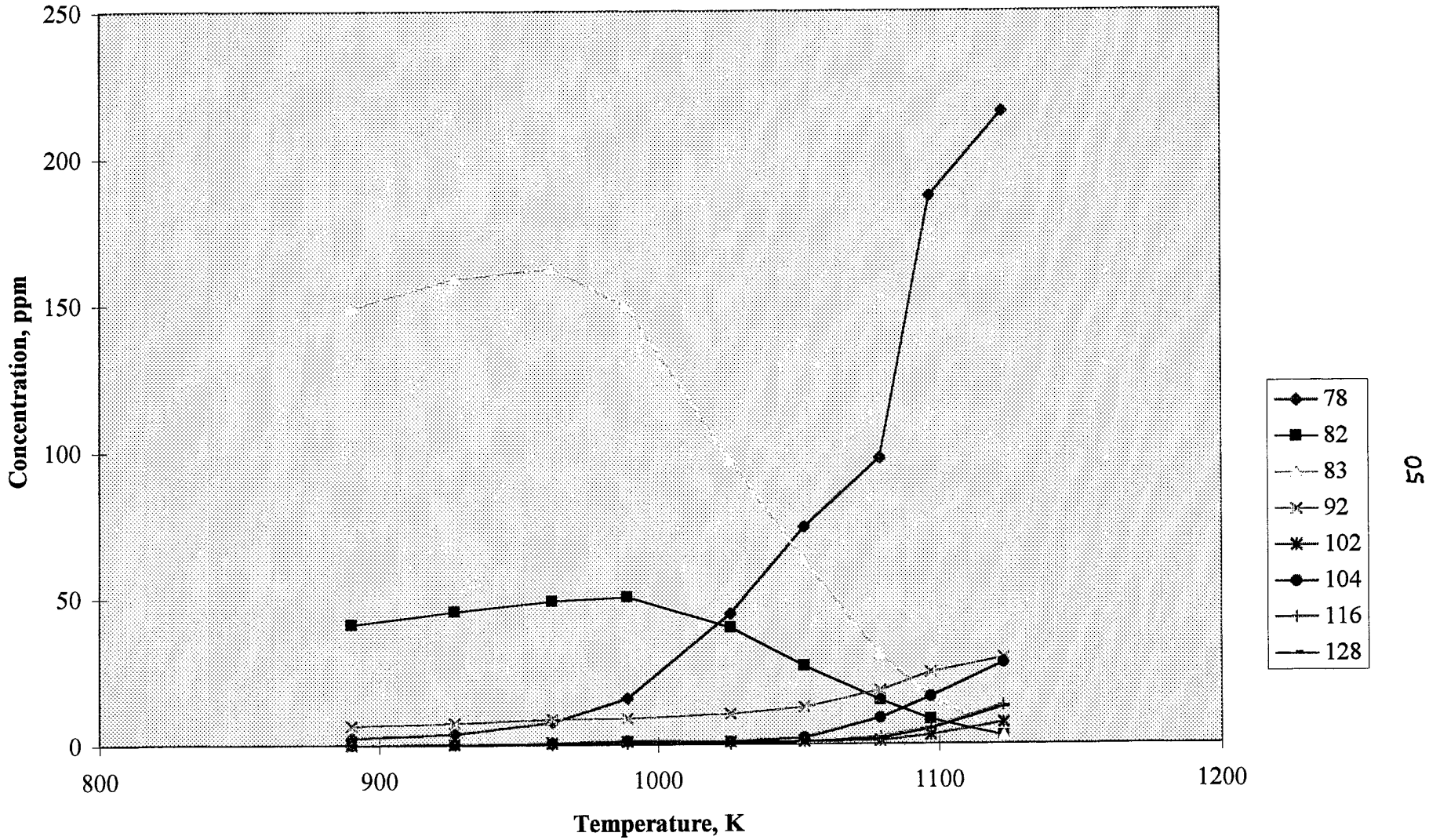

Figure 6: MCH pyrolysis, P=1400 torr, τ =50ms

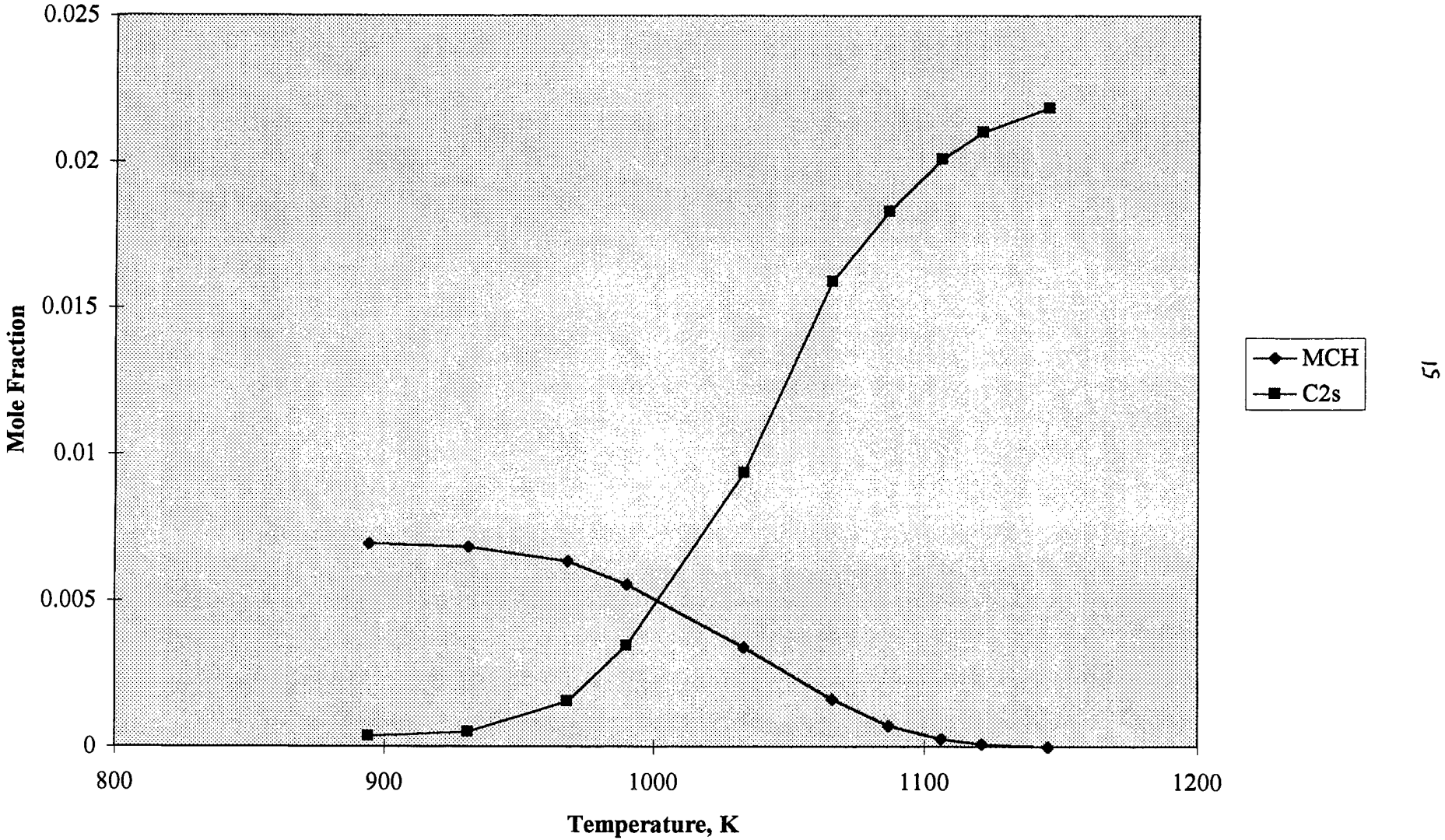

Figure 19: Mass 40-68 hydrocarbons formed during MCH pyrolysis, P=1400 torr, τ =50ms

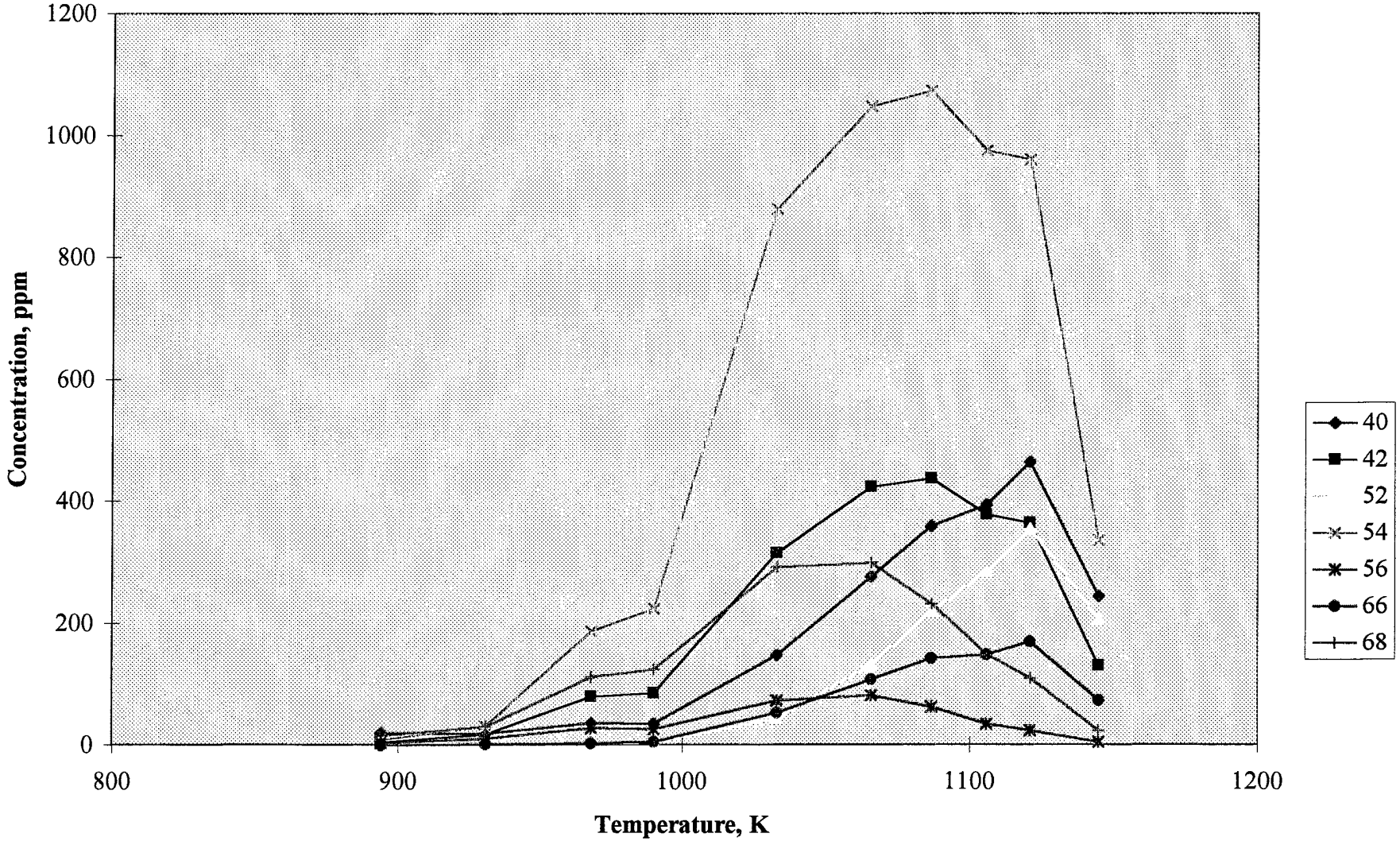

Figure20: Higher hydrocarbons formed during MCH pyrolysis, P=1400 torr, τ =50ms

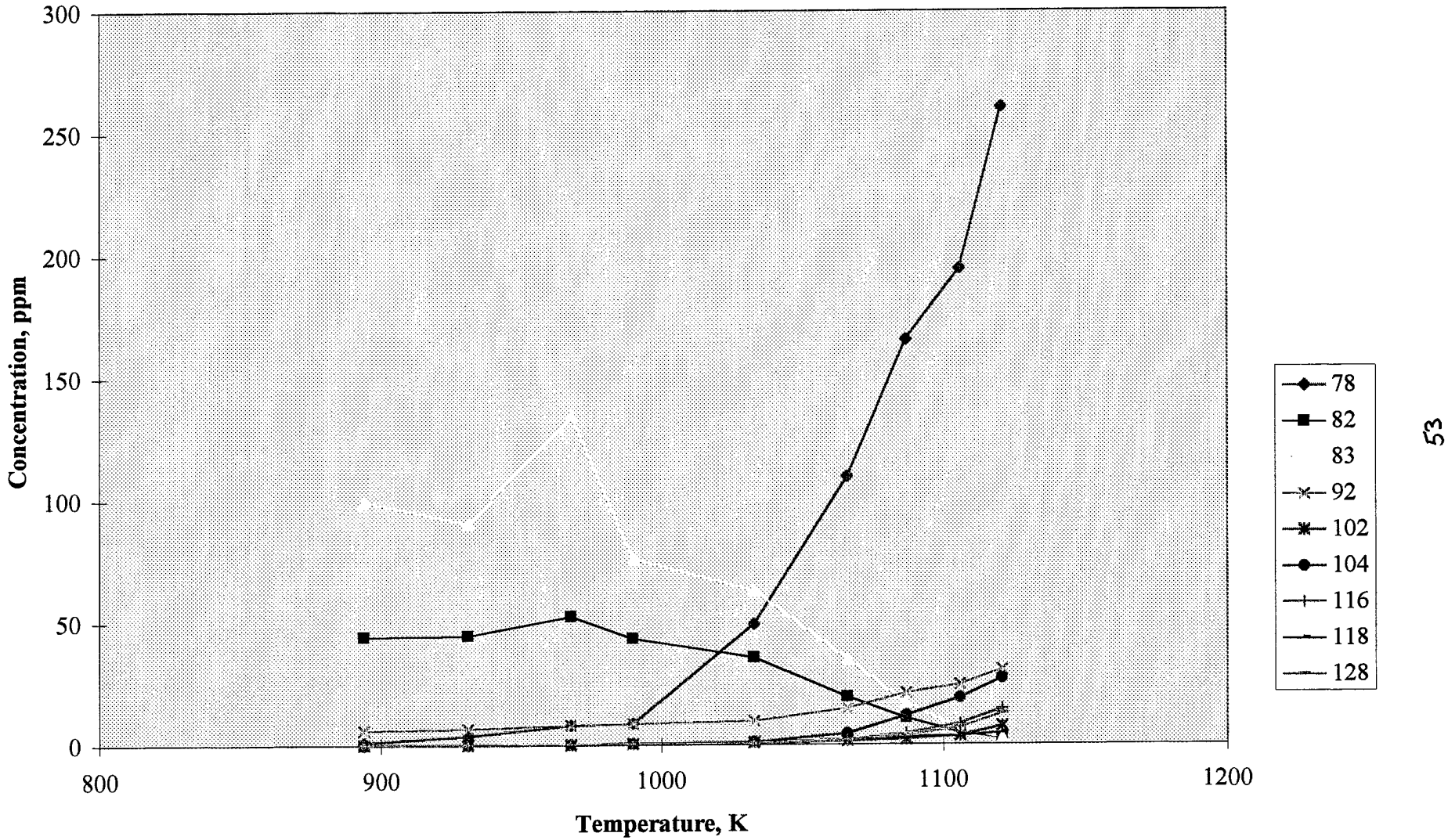

Centerline Phenylacetylene (C8H6)
(Parts Per Million)
Pure CH4
CH4 + Benzene
CH4 + Toluene
CH4 + Ethylbenzene
CH4 + Styrene
CH4 + Phenylacetylene
400
350
300
250
200
150
100
50
0
10
15
20
25
30
35
Height Above Burner; Z (Millimeters)

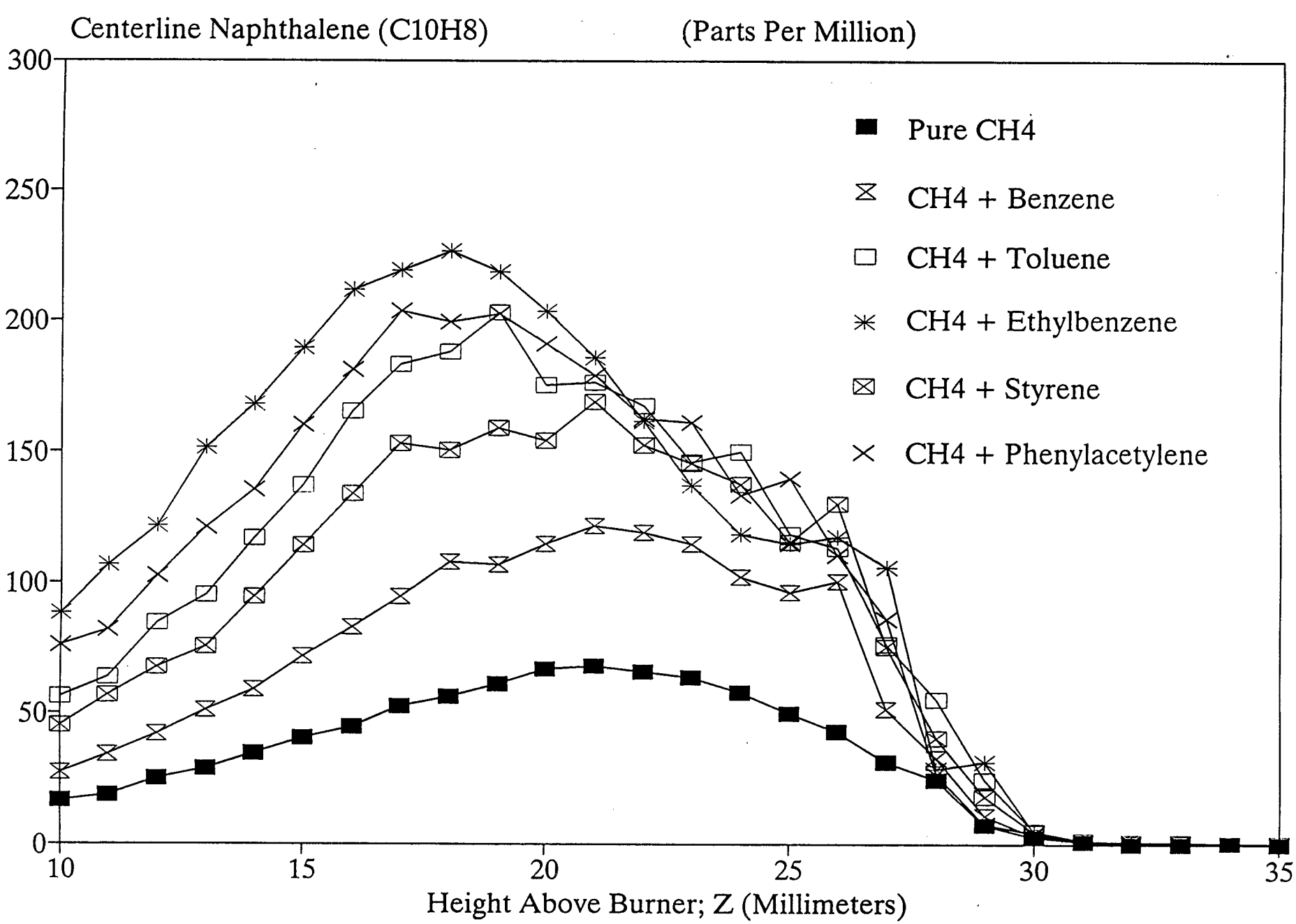
Centerline Naphthalene (C10H8)
(Parts Per Million)
300
250
200
150
100
50
0
10
15
20
25
30
35
Height Above Burner; Z (Millimeters)
Pure CH4
CH4 + Benzene
CH4 + Toluene
CH4 + Ethylbenzene
CH4 + Styrene
CH4 + Phenylacetylene

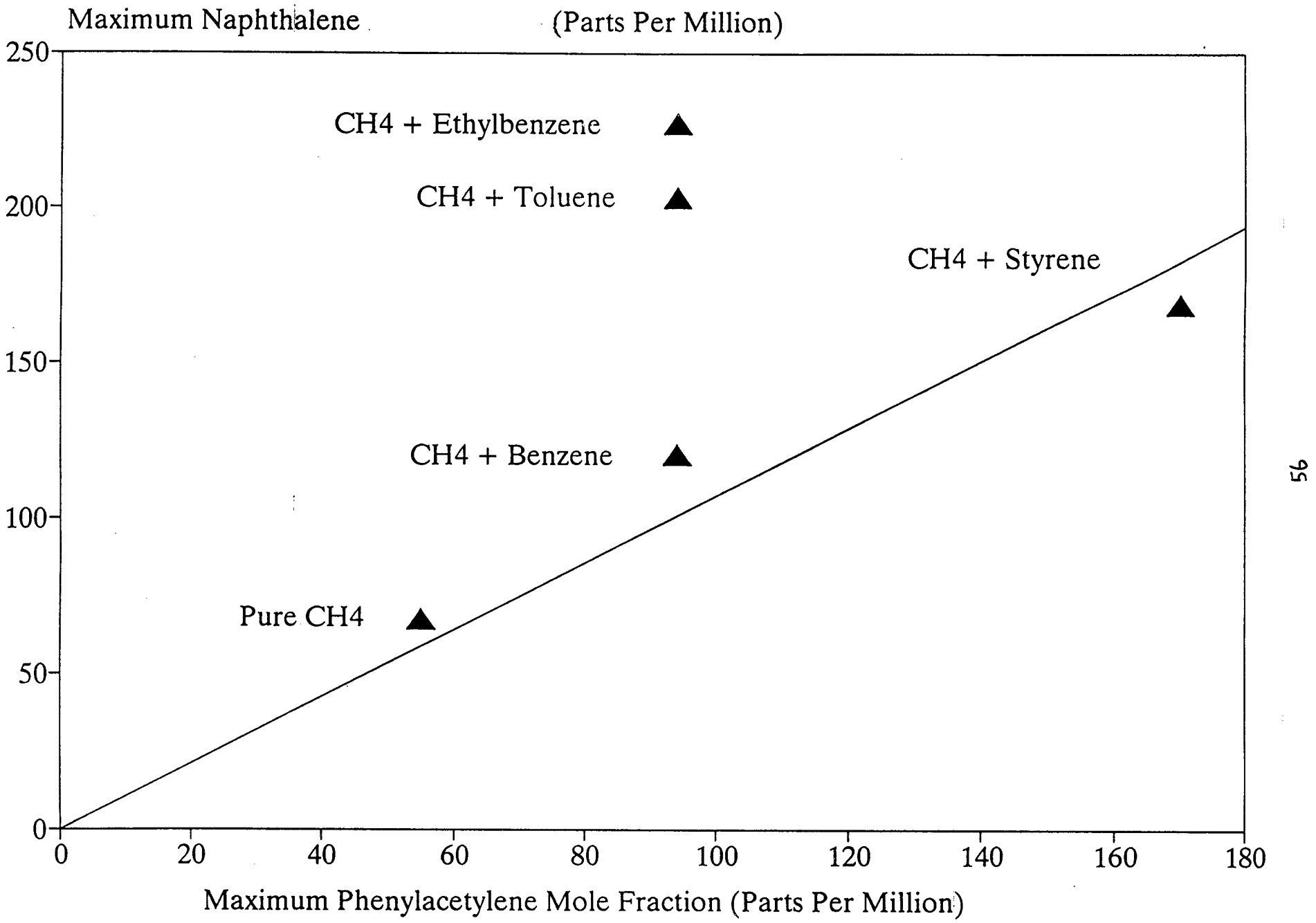
Maximum Naphthalene (Parts Per Million)
250
200
150
100
50
0
CH4 + Ethylbenzene
CH4 + Toluene
CH4 + Styrene
CH4 + Benzene
Pure CH4
0
20
40
60
80
100
120
140
160
180
Maximum Phenylacetylene Mole Fraction (Parts Per Million)

Personnel Supported:

Theodore W. Randolph - P.I.
Lisa D. Pfefferle - P.I.

Yan Chai - Post-doctoral worker
Charles McEnally - Post-doctoral worker
Sriram Natarajian - Graduate Student

Shankar Ganapathy- Graduate Student

Papers Citing AFOSR Support:

deGrazia, J., O'Brien, J.A., and Randolph, T.W., (1997) "Solute Rotational Dynamics in a Supercritical Fluid Revisited," *J. Phys. Chem.*, in press.

McEnally, C.S., and Pfefferle, L.D. "Experimental Assessment of Naphthalene Formation Mechanisms in a Non-Premixed Flame." *Combustion and Flame,* 128:545-558 (1998).

Natarajan, S., and Randolph, T.W., (1997) "Ultrasonic Velocity Measurements in Supercritical Jet Fuel," *J. Supercritical Fluids*, **10**, 65-70.

Ganapathy, S., O'Brien, J.A., and Randolph, T.W., "Molecular Simulation and EPR Studies of Rapid Bimolecular Reactions in Supercritical Fluids," *International Journal of Thermophysics*, vol. 17, No. 2, 471-481, 1996.

McEnally, C.S., and Pfefferle, L.D. "Aromatic and Linear Hydrocarbon Concentration Measurements" *Combustion Science and Technology,* 116-117:183-209 (1996).

Ganapathy, S., Randolph, T.W., and O'Brien, J.A., "Do Solute-Solute Interactions Affect Activation Limited Reactions? A Brownian Dynamics Study," *J. Supercritical Fluids*, vol. 9, 1996.

Ganapathy, S., Carlier, C., Randolph, T.W., and O'Brien, J.A., "The Influence of Local Structural Correlations on Free Radical Reactions in Supercritical Fluids: A Hierarchical Approach," *I&EC Res.*, 35, vol. 1, p. 19, 1996.

Ganapathy, S., O'Brien, J.A., and Randolph, T.W., "Effect of Solute-Solute Correlations on Rapid Reactions in Supercritical Fluids," *AIChE J.*, 11(2), 346-356, 1995.

Presentations and Interactions

1. AIChE Annual Meeting, Los Angeles, CA., Nov, 1997, "Solvent Effects on Rotational Diffusion and Reaction Rates in Supercritical Carbon Dioxide."

2. Annual Meeting of the AIChE, Chicago, November, 1996, "Ultrasound Velocity Measurements in Supercritical Fluids."

3. "Free Radical Reactivities in Supercritical Fuels: Experimental and Computational Studies" presented at the Center for Combustion Research, University of Colorado, Bolder, September 11, 1995.

4. "Reactions in Supercritical Fluids: Experiment and Molecular Simulation," National Institute of Materials and Chemical Research, Tskuba, Japan, February, 1995.

5. "Reactions in Supercritical Fluids: Experiment and Molecular Simulation," Department of Chemistry, University of Tokyo, Tokyo, Japan, February, 1995.

6. "Reactions in Supercritical Fluids: Experiment and Molecular Simulation," Department of Chemistry, University of Kyoto, Kyoto, Japan, February, 1995

7. "Higher Hydrocarbon Formation"Int'l Symposium on Toxic Combustion Byproducts, Berkeley, CA, June, 1995.

8. "Reactions in Supercritical Fluids: Experiment and Molecular Simulation" presented at the Department of Chemistry and Biochemistry, University of Colorado, Boulder, CO, April 12, 1995.

9. "Free Radical Reactions in Supercritical Ethane: Experiment and Computation," presented at the Department of Chemical Engineering, University of Arizona, November 29, 1994.

10. "Molecular Simulation and EPR Studies of Rapid Biomolecular Reactions in Supercritical Fluids," presented at the AIChE Annual Meeting, San Francisco, CA, November 14, 1994.

11. "Computational and Experimental Studies of Reactivities in Supercritical Fluids," presented at the Department of Chemical Engineering, University of Texas, Austin, November 8, 1994.

12. "Free Radical Reactions in Supercritical Fluids," presented at the Department of Agricultural and Chemical Engineering, Colorado State University, Ft. Collins, CO, October 28, 1994.

13. "Molecular Simulation and EPR Studies of Rapid Bimolecular Reactions in Supercritical Fluids," 12th Symposium on Thermophysical Properties, Boulder, CO, June 20, 1994.

14. "EPR Probes of Supercritical Fluid Reactivities" presented at the Department of Chemistry, Denver University, Denver, CO, April 28, 1994.

Conversation by Pfefferle with UTRC about interactions with Randolph on predicting supercritical fuel properties

Patents

No patents were applied for or anticipated. The detail circuit design for the ultra-sound instrument is available on request.

Honors/Awards

(TWR) "Invited Foreign Researcher," Japanese Agency of Industrial Science and Technology.